Marine Geology 352 (2014) 426–450

Contents lists available at ScienceDirect

Marine Geology

journal homepage: www.elsevier.com/locate/margeo

Establishing a new era of submarine volcanic observatories: Cabling Axial Seamount and the Endeavour Segment of the Juan de Fuca Ridge

Deborah S. Kelley [a,*], John R. Delaney [a], S. Kim Juniper [b]

[a] University of Washington, School of Oceanography, Seattle, WA 98195, United States
[b] University of Victoria, Ocean Networks Canada, Victoria, BC V8W 2Y2, Canada

ARTICLE INFO

Article history:
Received 10 July 2013
Received in revised form 4 March 2014
Accepted 6 March 2014
Available online 20 March 2014

Keywords:
submarine volcanoes
hydrothermal vents
Juan de Fuca Ridge
Endeavour Segment
Axial Seamount
cabled observatories

ABSTRACT

At least 70% of the volcanism on Earth occurs along the 65,000 km network of mid-ocean ridge (MOR) spreading centers. Within these dynamic environments, the highest fluxes of heat, chemicals, and biological material from the lithosphere to the hydrosphere occur during volcanic eruptions. However, because underwater volcanoes are difficult and expensive to access, researchers are rarely, if ever, in the right place at the right time to characterize these events. Therefore, our knowledge is limited about the linkages among hydrothermal, chemical and biological processes during seafloor formation and crustal evolution. To make significant advancements in understanding the evolution of MOR environments, the United States and Canada have invested in the first plate-scale submarine cabled observatory linked through the global Internet. Spanning the Juan de Fuca tectonic plate, these two networks include >1700 km of cable and 14 subsea terminals that provide 8–10 kW power and 10 Gbs communications to hundreds of instruments on the seafloor and throughout the overlying water column — resulting in a 24/7/365 presence in the oceans. Data and imagery are available in real- to near-real time.

The initial experimental sites for monitoring volcanic processes include the MOR volcanoes called Axial Seamount and the Endeavour Segment that are located on the Juan de Fuca Ridge. Axial, a hot-spot influenced seamount, is the most robust volcano along the ridge rising nearly 1400 m above the surrounding seafloor and it has erupted twice in the last 15 years. In contrast, the Endeavour Segment is characterized by more subdued topography with a well defined axial rift and it hosts one of the most intensely venting hydrothermal systems known. A non-eruptive spreading event lasting 6 years was documented at Endeavour between 1999 and 2005. Hydrothermal venting intensity, chemistry, and temperature, as well as associated biological communities at both sites were significantly perturbed by the magmatic and intrusive events. This paper presents the similarities and differences between the Axial and Endeavour volcanic systems and identifies reasons why they are ideal candidates for comparative studies. The U.S. has made a 25-year commitment for sustained observations using the cabled infrastructure. The highly expandable nature of submarine optical networking will allow for the future addition of novel experiments that utilize ever evolving advancements in computer sciences, robotics, genomics and sensor miniaturization. Comprehensive modeling of the myriad processes involved will continue to assimilate and integrate growing databases yielding a new understanding of integrated processes that create the seafloor in the global ocean basins.

Published by Elsevier B.V.

1. Transforming studies of volcanoes, hot springs, and life

For four billion years submarine volcanism has impacted the global oceans, driving hot spring systems that not only influence the chemistry of the ocean, but which also support some of the most novel organisms on Earth (Davis and Elderfield, 2004; Wilcock et al., 2004). Approximately 70% of the volcanism on the planet occurs beneath the ocean's surface, with much of the activity focused along the 65,000 km-long mid-ocean ridge (MOR) spreading system. Although, the associated hydrothermal vent ecosystems were initially viewed as isolated, widely-spaced oases on an otherwise barren seafloor, in the past three decades the discovery rate of vent sites has dramatically increased in response to maturation of search strategies and improved detection techniques: more than 300 vent sites have now been documented with evidence of many more in the global oceans (Fig. 1).

On-going discoveries about these remarkable environments continue to astound us, from the chemical and physical nature of black smokers and hydrothermally active fissure systems, to the multitude of highly-adapted life forms thriving within these extreme environments. Striking examples include the discovery of the 350 °C black smoker 'Godzilla' on the Endeavour Segment of the Juan de Fuca Ridge, which in 1995 stood as high as a 15-story building, towering

* Corresponding author.

http://dx.doi.org/10.1016/j.margeo.2014.03.010
0025-3227/Published by Elsevier B.V.

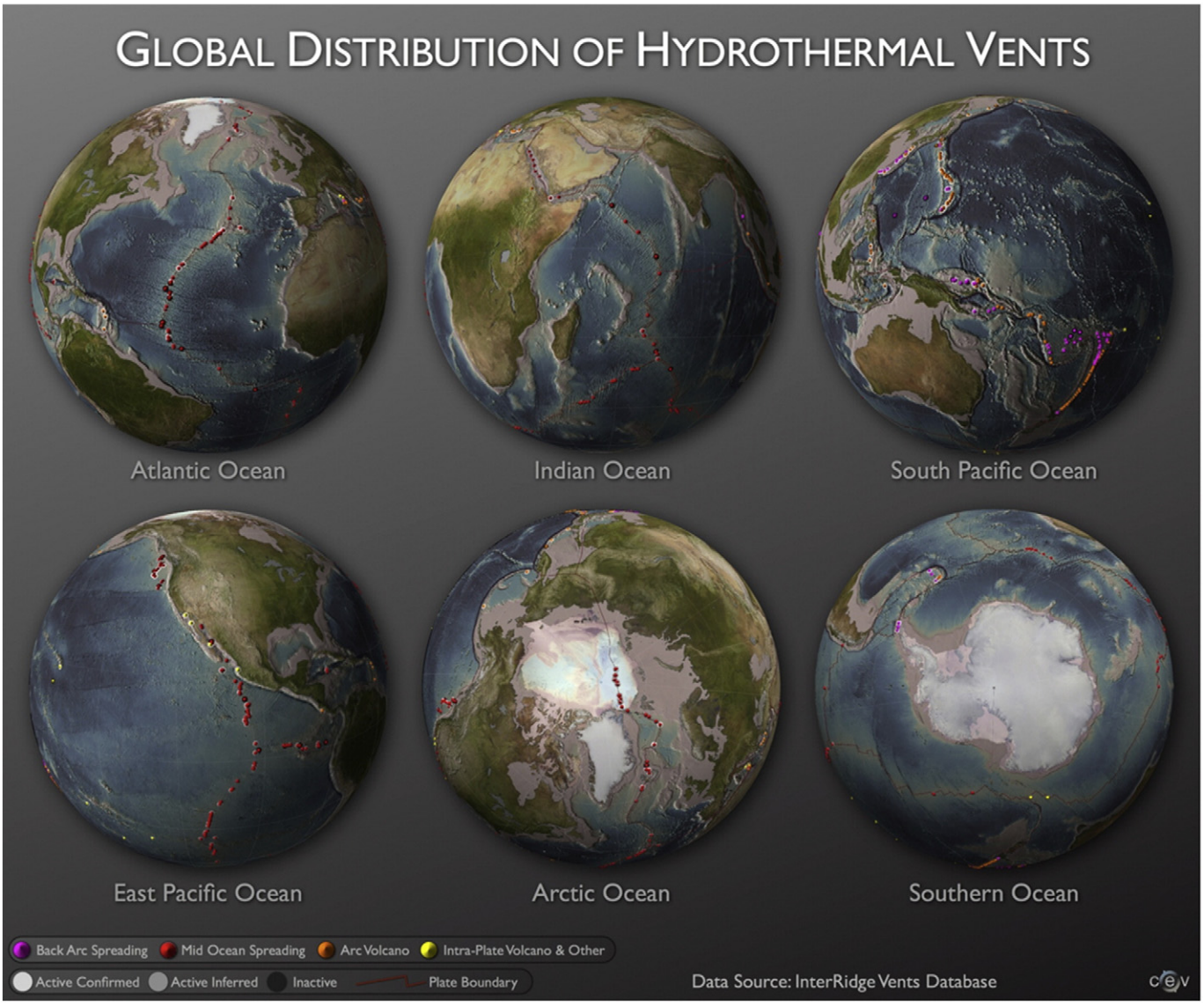

Fig. 1. Global distribution of hydrothermal vents based on the InterRidge vent database (http://www.interridge.org/Irvents). Image produced by the Center for Environmental Visualization, University of Washington.

over the surrounding volcanic terrain (Robigou et al., 1993). In 1999, one of the highest temperature organisms on Earth, capable of surviving at temperatures 121 °C, was cultured from 1-year old black smoker material recovered from the Endeavour (Kashefi and Lovley, 2003). In 2000, a completely different type of hydrothermal system was serendipitously discovered on the Mid-Atlantic Ridge called the Lost City Hydrothermal Field, hosting actively venting limestone chimneys that rise 60 m above the seafloor (Kelley et al., 2001a, 2005). Equally surprising, in 2004 and 2010, shallow volcanic calderas in the Mariana arc and volcanoes in Lau Basin were discovered hosting pools of molten sulfur (Embley et al., 2006; Lupton et al., 2006) and explosive lava bubbles (Resing et al., 2011). Perhaps the most far-reaching of these discoveries, however, is that life itself may have originated within these dynamic systems in which geological, chemical, and biological processes are intimately linked (Baross and Hoffman, 1985; Martin et al., 2008; Langmuir and Broecker, 2012).

Although significant progress has been made in understanding process linkages in these dynamic environments, further scientific advances are increasingly dependent on our ability to collect long-term, high-frequency observations using diverse networks of platforms, sensors, and samplers that are in the right place at the right time to capture the events/processes of interest. Distributed sensor networks in terrestrial environments, which provide real-time documentation about the environment and human activities are now widespread and accessible to a global audience via the Internet. However, similar capabilities in the oceans are extremely rare, leaving many of the significant seafloor processes poorly characterized, particularly in both the time domain and at the required spatial scales.

The major volcanic and tectonic processes that create the oceanic crust and modulate heat, chemical, and biological fluxes through the seafloor are inherently episodic on decadal timescales, but they are also punctuated by short-lived and frequent events. For example, water column analyses above recently erupted submarine volcanoes show that significant heat, chemicals, and biological material are ejected into the overlying ocean during the formation of megaplumes and following eruptive events (Embley et al., 1991; Haymon et al., 1991; Baker et al., 1995; Lupton, 1995; Delaney et al., 1998; Kelley et al., 1998; Lupton et al., 1999; Lilley et al., 2003; Baker et al., 2004; Meyer et al., 2013). The megaplumes are characterized by anomalous heat-helium content and are enriched in hydrogen and methane (Kelley et

al., 1998). They also have elevated manganese and iron concentrations with respect to ocean background water (Lupton, 1995; Murton et al., 2006; Baker et al., 2012). The buoyant plumes can rise a thousand meters or more above the surrounding seafloor, they can be 20 km across, and 70 km in length (Baker et al., 1987; Lupton, 1995; Lupton et al., 1999; Murton et al., 2006). It is likely that they form extremely rapidly, perhaps on the order of a few hours (Lavelle, 1995). The rising fluids contain novel subseafloor thermophilic microorganisms, injected into the overlying ocean as crustal fluids are flushed from depth (Delaney et al., 1998; Summit and Baross, 1998, 2001; Meyer et al., 2013). Subsequent to formation, the megaplumes are wafted away from the ridge axis by ocean currents. Modeling results indicate that megaplumes may have lifetimes of years (D'Asaro et al., 1994; Carazzo et al., 2013), however, monitoring of individual plumes over their life span has never been achieved.

Diking and volcanic eruptive events also significantly perturb existing hydrothermal systems (Butterfield et al., 1997; Von Damm, 2000; Lilley et al., 2003; Fornari et al., 2012), causing drastic changes in vent fluid chemistry and temperature. Rapid changes in heat and volatile fluxes also occur with injection of volatiles (e.g. CO_2) over a few month period that may rival that released by a mature hydrothermal system over an entire year (Lilley et al., 2003). Perhaps even more profound, however, is the formation of "snowblowers" that result from the effusion of crustal fluids with massive microbial biomass that vent into the hydrosphere following seafloor diking–eruptive events (Haymon et al., 1991; Delaney et al., 1998; Holden et al., 1998; Summit and Baross, 1998; Proskurowski et al., 2012; Meyer et al., 2013). These observations along with documentation of high numbers of microbes thriving within low- to moderate-temperature diffuse flow fluids have been instrumental in forming the hypothesis that a vast, but unexplored, microbial biosphere exists in the crust in close proximity to volcanoes and active submarine hydrothermal systems (Gold, 1992; Delaney et al., 1998; Wilcock, 2004; Huber et al., 2007).

In 1987, it was recognized that while expedition-based exploration and study of these dynamic systems would always be important, the only way to capture these high impact events would be to maintain long-term, real-time monitoring and response capabilities at a number of sites with high probability for magmatic and/or tectonic activity. From this recognition, the concept of installing high-power and high-bandwidth underwater cabled observatories emerged. These first conceptual arrays focused on highly energetic Earth and ocean processes operating in shallow coastal waters off of Washington, Oregon, and British Columbia and extending out to the Juan de Fuca spreading center (Delaney et al., 1987, 1988). In the early 1990s, a consortium was formed between the U.S. and Canada to develop a plate-scale submarine electro-optically cabled ocean observatory in the northeast Pacific. The partnership evolved to include a Canadian cabled array that would cover the northern 1/3 of the Juan de Fuca Plate and a U.S. system that would instrument the central and southern 2/3 of the plate (Fig. 2). In concert, this plate-scale cabled observatory was called NEPTUNE (Northeast Pacific Time Series Underwater Networked Experiment) (e.g., Delaney et al., 2000).

This effort is now being realized: in 2014 the plate-scale cabled observatory will be fully installed. The project is an international collaborative effort involving the National Science Foundation's (NSF) Ocean Observatory Initiative (OOI) and Ocean Networks Canada (Fig. 2). Infrastructure to specifically address MOR processes is focused on Axial Seamount (the largest and most active volcano on the Juan de Fuca Ridge), and the Endeavour Segment (one of the most hydrothermally-active sites along the global MOR spreading network) (Fig. 3).

These two observatories, integrated through the Internet, include ~1700 km of cable and 14 subsea terminals called Primary Nodes that

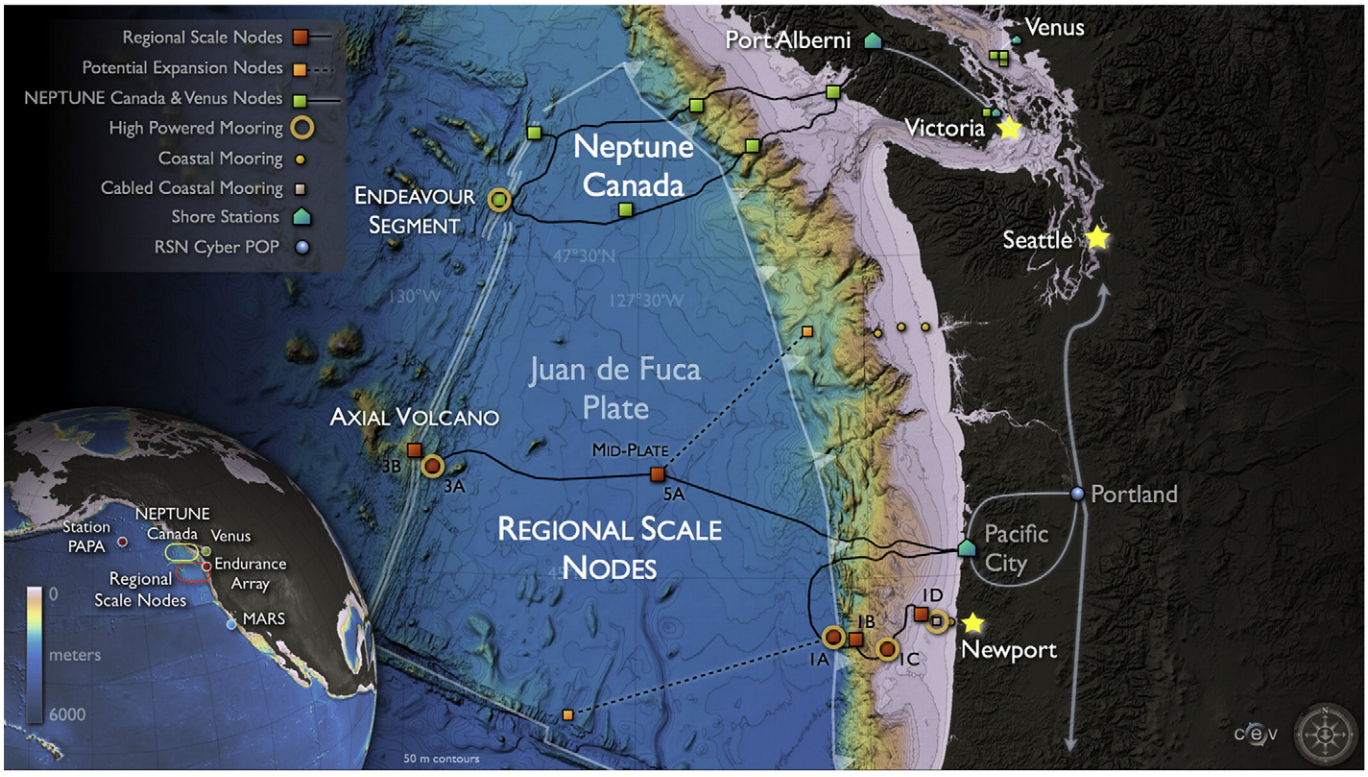

Fig. 2. Map showing the location of the U.S. submarine cabled observatory called the Regional Scale Nodes, and the Canadian observatory called Neptune Canada. The two systems include 1700 km of telecommunication-grade cables enhanced with high power capabilities (8–10 kW) and communication bandwidth at 10 Gbs. Terrestrial shore stations at Pacific City, Oregon and at Port Alberni, Vancouver Island connect the submarine backbone system to shore where it feeds into the Internet. In addition to myriad seafloor sensors, the two cabled observatories include water column moorings, which on the RSN rise nearly 2700 m into the overlying water column, hosting two instrumented profilers.

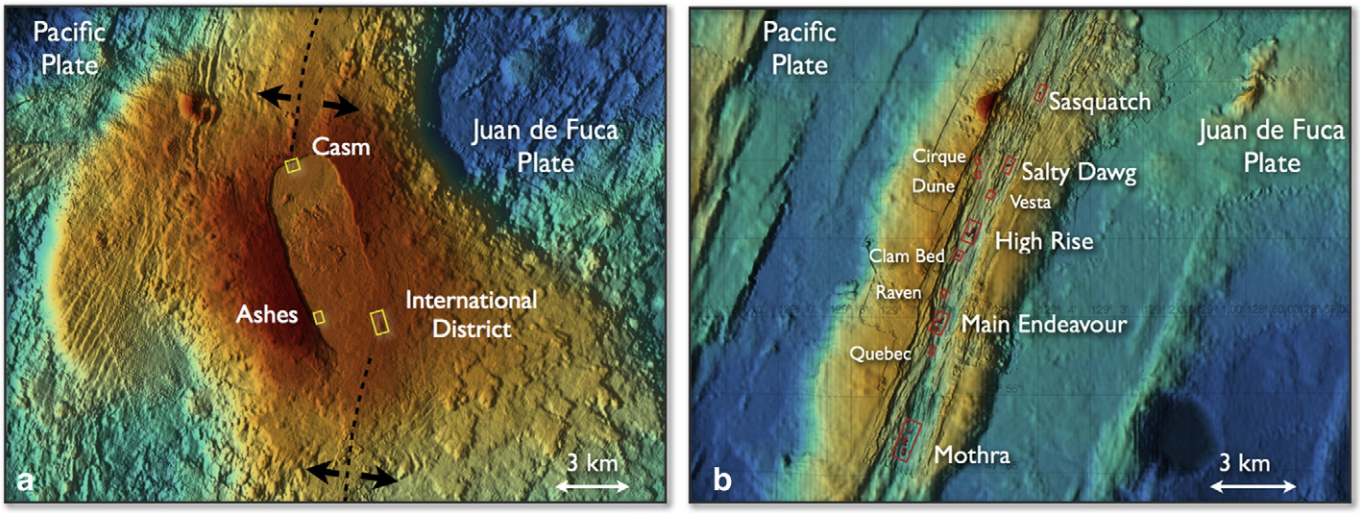

Fig. 3. a) Axial Seamount, on the Juan de Fuca Ridge, rises from a water depth of ~2700 m (dark blue) to 1500 m (red orange) over a distance of ~25 km. The caldera is centered at ~130°W and 45°58′N. It is the most volcanically active volcano on the ridge, and hosts three main hydrothermal fields (Ashes, CASM, and International District), as well as myriad diffuse flow sites. The summit is dissected by the spreading center (dashed lines) and is marked by a large caldera that is ~3 km across and 9 km in length. b) In contrast to the pronounced topographic high of Axial Seamount, the Endeavour Segment is characterized by a narrow rift valley, which in the central portion of the segment is at a water depth of ~2200 m. It hosts at least five hydrothermal fields (e.g. Mothra and Main Endeavour), and several diffuse flow fields (e.g. Quebec, Dune, and Clam Bed). It is one of the most active hydrothermal systems known on the global mid-ocean ridge system. The Main Endeavour Field is located at ~47°57′N, 129°06′W.

provide power and communication to key experimental sites. When fully installed in 2014, they will host myriad smaller junction boxes and thousands of meters of extension cables connected to hundreds of seafloor and water column instruments. The high power (up to 10 kW) and 10 Gbs fiber-optic cables provide continuous, real-time, two-way communication and pulse per second timing to moored and seafloor sensors, instrumented wire crawlers, and seafloor robots with direct connection to the Internet.

This paper provides an overview of the cutting edge infrastructure that comprises the observatories and what is known about some of the dynamic processes operating at Axial Seamount and the Endeavour Segment. Example goals of the cabled observatories include:

Fig. 4. Locations of installed (green dots) and planned cabled seafloor observatories (red dots). Many of the sites located around the perimeter of Europe are part of the extensive ESONET (European Sea Floor Observatory Network) array planned to include 5000 km of submarine fiber optic cables (http://www.oceanlab.abdn.ac.uk/research/esonet.php). Also shown are the locations of high latitude uncabled mooring arrays (Papa, Irminger, Southern Ocean, Argentine basin), the coastal arrays (Pioneer, Washington and Endurance Lines) that are components of the NSF's Ocean Observatories Initiative.

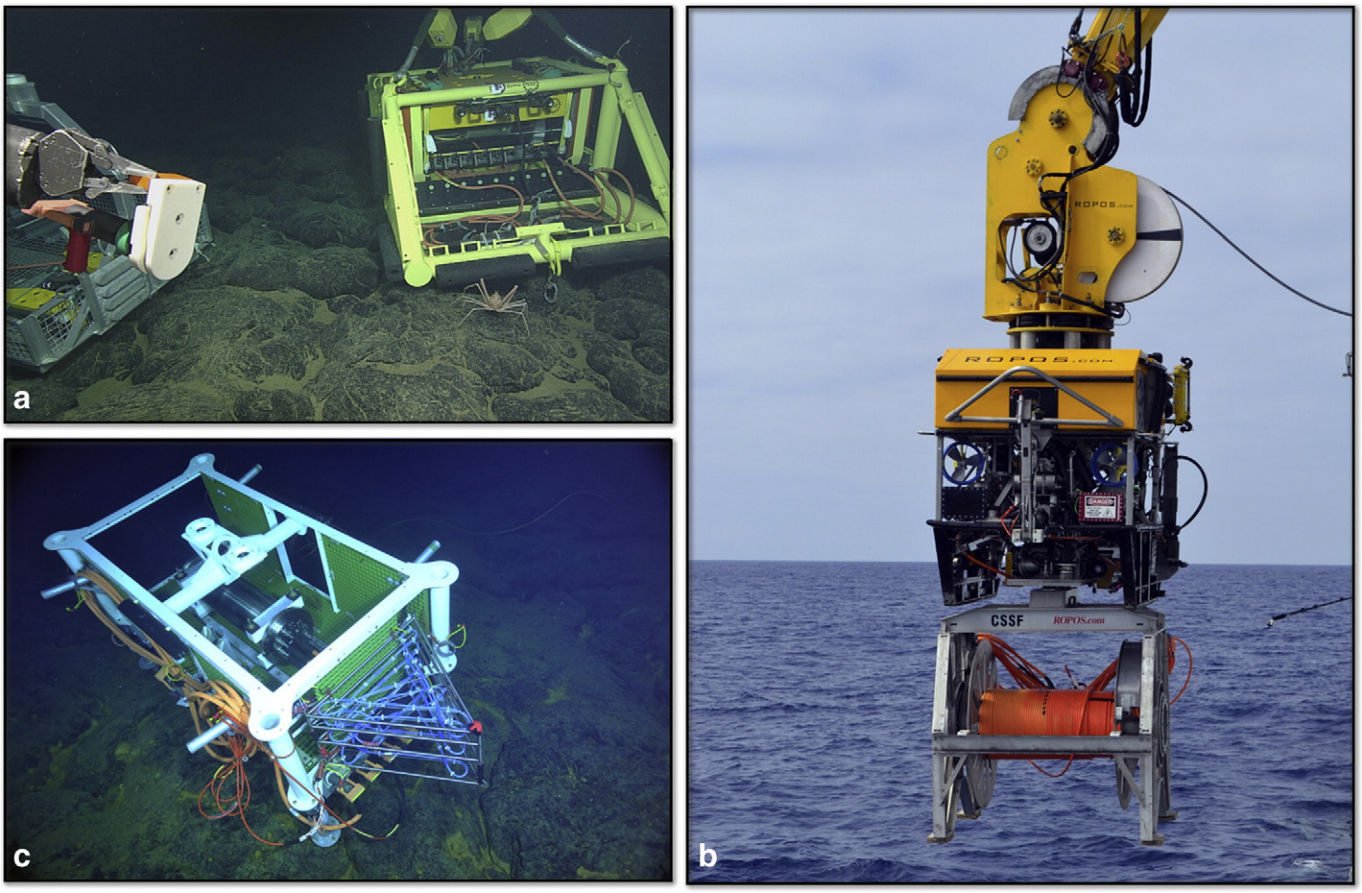

Fig. 5. Primary and secondary infrastructure for the cabled observatories. a) Primary Node 3B at the summit of Axial Seamount. The orange fiber optic cables are connected to power and communication ports by underwater wetmate connectors. One of the arms of the Canadian *ROV ROPOS* is shown to the left. b) The *ROV ROPOS* with the Remotely Operated Cable Laying System mounted on its underbelly takes extension cables down to the seafloor to be installed. It is operated by the Canadian Scientific Submersible Facility (CSSF). c) A medium-powered Junction Box installed in the ASHES hydrothermal field on Axial Seamount in 2013. A 3D thermistor array awaits deployment at the hydrothermal vent called Mushroom (see Fig. 15). a) Image courtesy of OOI-NSF/UW/CSSF. c) Image courtesy of OOI-NSF/UW/CSSF.

- to monitor melt migration beneath spreading centers and crustal deformation with implications for eruptive cycles and spreading processes;
- to characterize and quantify the immediate biological, chemical and geological consequences of transient events such as dike intrusions, eruptions, and deformation events associated with seafloor spreading;
- to make direct long-term measurements of seafloor inflation with concomitant seismic and hydrothermal volatile measurements, which may lead to predictive capabilities for seafloor eruptions;
- to quantify temperature, chemical, and biological parameters within hydrothermal and eruptive effluent (e.g. megaplumes) and to begin to quantify heat and chemical fluxes; and
- to make long-term, co-registered measurements of biological communities in and around hydrothermal vents to characterize their diversity, productivity, temporal and spatial distributions, and their response to changing environmental conditions.

Two-way communication to seafloor and water column instruments, seafloor crawlers, and water column profilers throughout full ocean depths will allow highly interactive rapid responses to diking events, volcanic eruptions, and earthquakes and co-registered real-time measurements of associated changes in venting and biological communities with capabilities to change data accumulation, fluid–DNA sampling rates, and camera look angles. In concert, these two systems will supply 25 years of sustained data flow with opportunities for continued development of innovative in situ sensing systems. New technologies will build on advanced cabled robot-sensor ensembles such as 'Wally' on Neptune Canada that can be controlled from continents away, making repeat photomosaics of benthic communities and co-registered environmental measurements. These benthic crawlers allow documentation of temporal changes in benthic seep ecosystems, methane concentrations, and seasonal environmental changes such as

Fig. 6. a) A bottom-pressure tilt instrument installed at the summit of Axial Seamount to measure seafloor inflation and deflation (Chadwick et al., 2012). b) A short-period seismometer installed in the eastern portion of the Axial caldera in 2013 by the *ROV ROPOS*. c) A resistivity (chlorinity)–temperature probe installed in the hydrothermal chimney called Escargo in the International District Hydrothermal Field in 2013. This battery-powered instrument will be replaced by a cabled sensor in 2014 to examine boiling processes. d) The Tempo-Mini cabled video camera system developed by IFREMER installed at the black smoker called 'Grotto' in the Main Endeavour Hydrothermal Field. e) The cabled instrument called COVIS (Cabled Observatory Vent Imaging System) deployed near Grotto. It detects turbulent fluctuations associated with warm, shimmering water, providing a sonar-generated "map" of diffuse flow (Rona and Light, 2011; Bemis et al., 2012). f) A cabled Remote Access Sampler (RAS) is deployed next to the Tempo-Mini camera system at Grotto. The nozzle leading from the RAS allows time-series intake of hydrothermal fluids into discrete sampling chambers. A RAS coupled to a DNA sampler will be deployed at the International District hydrothermal field in 2014, providing corresponding time-series analyses of temperature, fluid chemistry, and microbial DNA (Butterfield et al., 2004).
a) Image courtesy of OOI-NSF/UW/CSSF. b) Image courtesy of OOI-NSF/UW/CSSF. c) Image courtesy of OOI-NSF/UW/CSSF. d-f) Image courtesy of Ocean Networks Canada and CSSF.

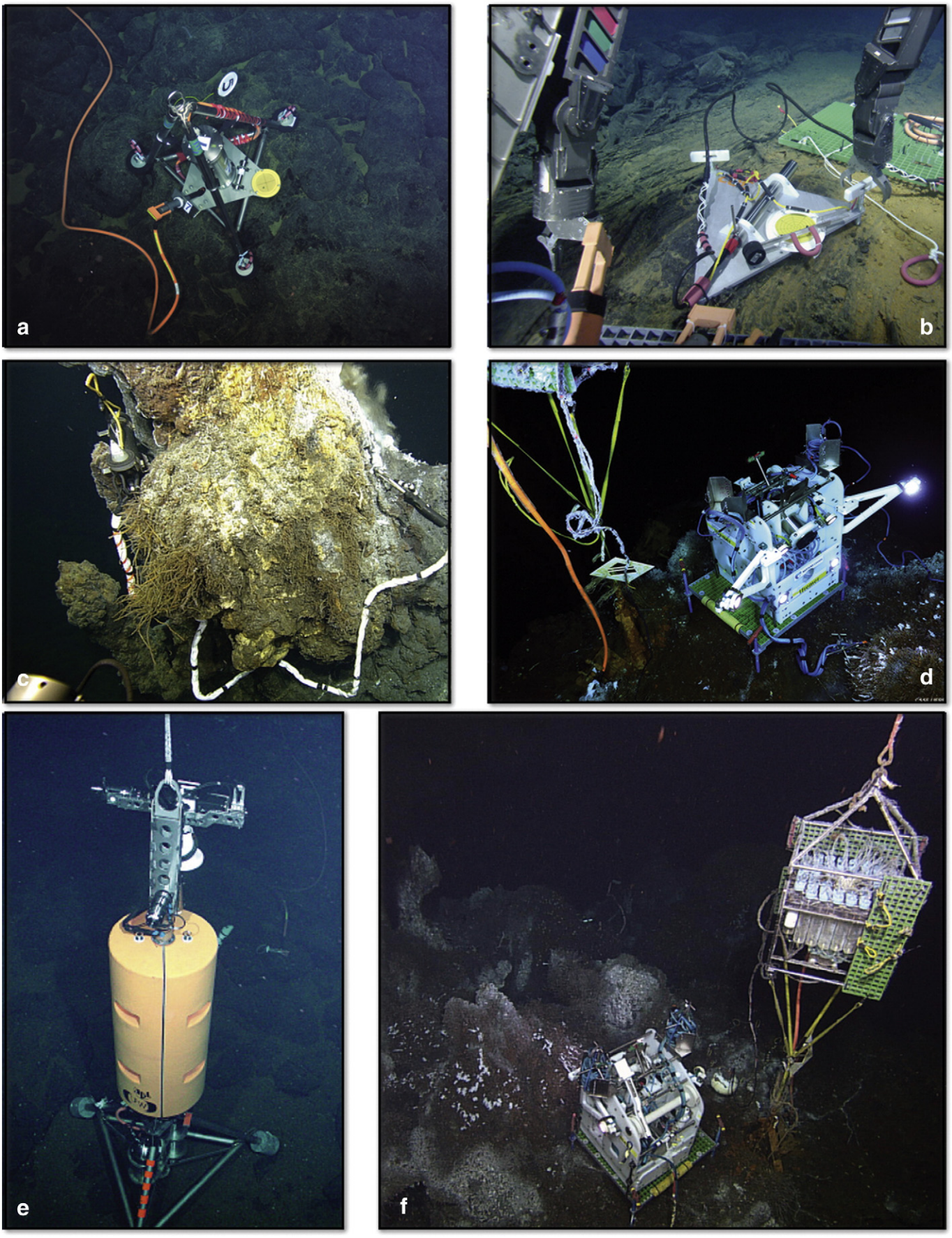
a
b
c
d
e
f

chlorophyll flux variation (Purser et al., 2013). Indeed, in situ genomic analyzers are now being developed for use on deep-sea cabled observatories (see http://www.mbari.org/ESP/esp_DEEP.htm; Scholin et al., 2009; Harvey, 2012). Although the integrated arrays are the first at a plate-scale, there are >15 cabled observatories now installed or planned within the global ocean (Fig. 4) (Delaney and Kelley, 2014; Favali et al., 2014). International installation of progressively advanced networked cabled seafloor observatories will provide unprecedented monitoring of the oceans, and the entrainment of a global community of users — researchers, educators, policy makers and the public.

2. Implementing the first plate-scale underwater observatory

In 2000, the Ocean Science Division of the NSF put forth a proposal for Major Research and Equipment Facility Construction (MREFC) funds from congress to incorporate the NEPTUNE cabled observing systems concept into an even broader ocean science program that included 1) high-latitude measurements of heat fluxes and greenhouse gas exchange at the air–sea interface with mooring arrays at Station Papa in the Gulf of Alaska, the Irminger Sea, Argentine Basin, and southwest of Chile; and 2) focused enquiries in critical coastal environments where populations are stressing near-shore oceanic systems, with mooring arrays off Newport, Oregon (Endurance Array — Oregon Line), Grays Harbor, Washington (Washington Line) (Fig. 2), and in the Northwest Atlantic off the coast of New England (Pioneer Array). Linking the marine assets is a Cyberinfrastructure component (CI) to provide infrastructure for data flow, management, and distribution, as well as observatory resource management. The entire program was named the Ocean Observatories Initiative (OOI — http://www.oceanobservatories.org/).

In 2003, NEPTUNE Canada led by the University of Victoria received federal funding through the Canada Foundation for Innovation, and from provincial and private funding to complete planning and implementation of its network on the northern portion of the Juan de Fuca Plate (http://neptunecanada.ca). With these funds, Alcatel–Lucent began installation of NEPTUNE Canada in the summer of 2007. Also in 2007, NEPTUNE U.S. was renamed the Regional Scale Nodes (RSNs) and the University of Washington (UW) became the Implementing Organization for the RSN. The UW was tasked with developing the design, fabrication and installation of the RSN, as well as operating the cabled network for the first two years subsequent to construction (http://oceanobservatories.org/).

NEPTUNE Canada began installing seafloor instruments in 2008 and data were made available online for the first time in February 2009 (http://www.oceannetworks.ca/). NEPTUNE Canada and the coastal VENUS cabled observatory were merged under the Ocean Networks Canada (ONC) umbrella in 2013; construction is now complete. Construction funds for the RSN were obtained in 2009 and L3 MariPro was awarded the contract for installation of the US portion of the observatory. Installation of the Primary Infrastructure was completed in 2012, and the entire RSN system will be completed in 2014 (http://interactiveoceans.washington.edu/). In total between these two systems, nearly $500 M of infrastructure will be deployed on the seafloor and throughout the water column. The two systems will be integrated through the ONC's Digital Infrastructure and the OOI Cyberinfrastructure, providing real-time access to anyone connected to the Internet.

2.1. Infrastructure to access the deep

The cabled assets include the Primary Infrastructure, which is comprised of modified telecommunication cables (backbone cables), repeaters, and 14 Primary Nodes that distribute power from two Shore Stations (Pacific City, Oregon and Port Alberni, Vancouver Island) to key sites along the Juan de Fuca plate (Figs. 2 and 5). All 1700 km of backbone cable has been installed, as well as the 14 Primary Nodes. The Shore Stations connect directly to terrestrial telecommunication fibers, providing access to the global Internet. Each Primary Node provides 8–10 kW of power, and 10 Gbs bandwidth at ocean depths as great as ~3000 m. Their main function is to distribute power and bandwidth to the Secondary Infrastructure, which includes junction boxes, extension cables, instruments, and moorings (Figs. 5–7). They also contain house-keeping functions of the system control, out-of-band communications, and engineering monitors. The entire Primary Infrastructure is monitored and controlled by a Network Management System (NMS) that allows the communication and power systems to be monitored for activity, status, utilization and it also allows controlled allocations of resources across the system (e.g., power). The NMS can be accessed from the Shore Stations or from remote facilities including the RSN Observatory Network Management Laboratory at the UW and the ONC Observatory Operations Centre at the University of Victoria.

To access specific experimental sites, low- to medium-power junction boxes (secondary nodes) are connected to the Primary Nodes by extension cables that can reach several kilometers in length (e.g., Fig. 5b). Each junction box includes eight sensor ports that can handle 12–48 V DC, with communication capabilities of 10/100 BASE-T, RS232, RS485, and 1-GigE and pulse per second timing (PPS and 1588) (Fig. 5c). Ports are configured predeployment to meet each instrument requirement. Each port can provide 50 to 200 W power. Expansion ports provide "daisy-chain" capabilities via extension cables to junction boxes, making the system highly expandable. Extension cables are of variable length (<10 m to >10 km), depending on the science requirements for the sensor locations. The cables are connected through either drymate or wetmate connectors: wetmate connectors are particularly valuable because they allow underwater connection with remotely operated vehicle (ROV), such that an instrument or cable can be recovered or deployed without having to bring up an entire junction box or Primary Node.

2.2. Platforms and instruments

The deep volcanic and hydrothermal environments at Axial Seamount and the Endeavour Segment are some of the most extreme on Earth and as such special platforms and instrumentation were needed to meet the scientific requirements (Figs. 5–7; Tables 1 and 2). These platforms include full to partial ocean depth water column moorings (~2800 m) with instrumented wire crawlers, platforms and winches (Figs. 2 and 7). The moorings are designed to measure global and local currents (e.g., flow over rough topography and internal waves), megaplumes and hydrothermal plumes, ocean chemistry (e.g., pH, CO_2, nutrients), heat flux, and biology (e.g., zooplankton distribution and chlorophyll). Examples of specialized seafloor sensors include real-time high definition video and digital still cameras that provide unprecedented views of macrofaunal and microbial assemblages at the vents and chemical sensors [e.g., temperature–resistivity–hydrogen (H_2) probes (as an analog for chlorinity), pH–hydrogen sulfide (H_2S)–H_2–temperature instruments, and mass spectrometers]. In concert, these sensors provide information on the environmental conditions (e.g., temperature distribution and volatile concentrations) in which the biological communities thrive. The instrumentation also yields information on the impact of flow perturbations associated with eruptive and seismic events on biological communities. Other sensors include broadband and short-period seismometers to monitor earthquake and subsurface magma migration, temperature and chemical probes in diffuse and black smoker sites, fluid and DNA samplers, and pressure-tilt meters for measurement of pre-eruptive inflation events and post-eruptive deflation (Table 2).

3. Two diverse volcanoes: Axial and Endeavour

Axial Seamount, and the Endeavour Segment of the intermediate-spreading Juan de Fuca Ridge were chosen as the first volcanic cabled observatory sites because they are dramatically different in their

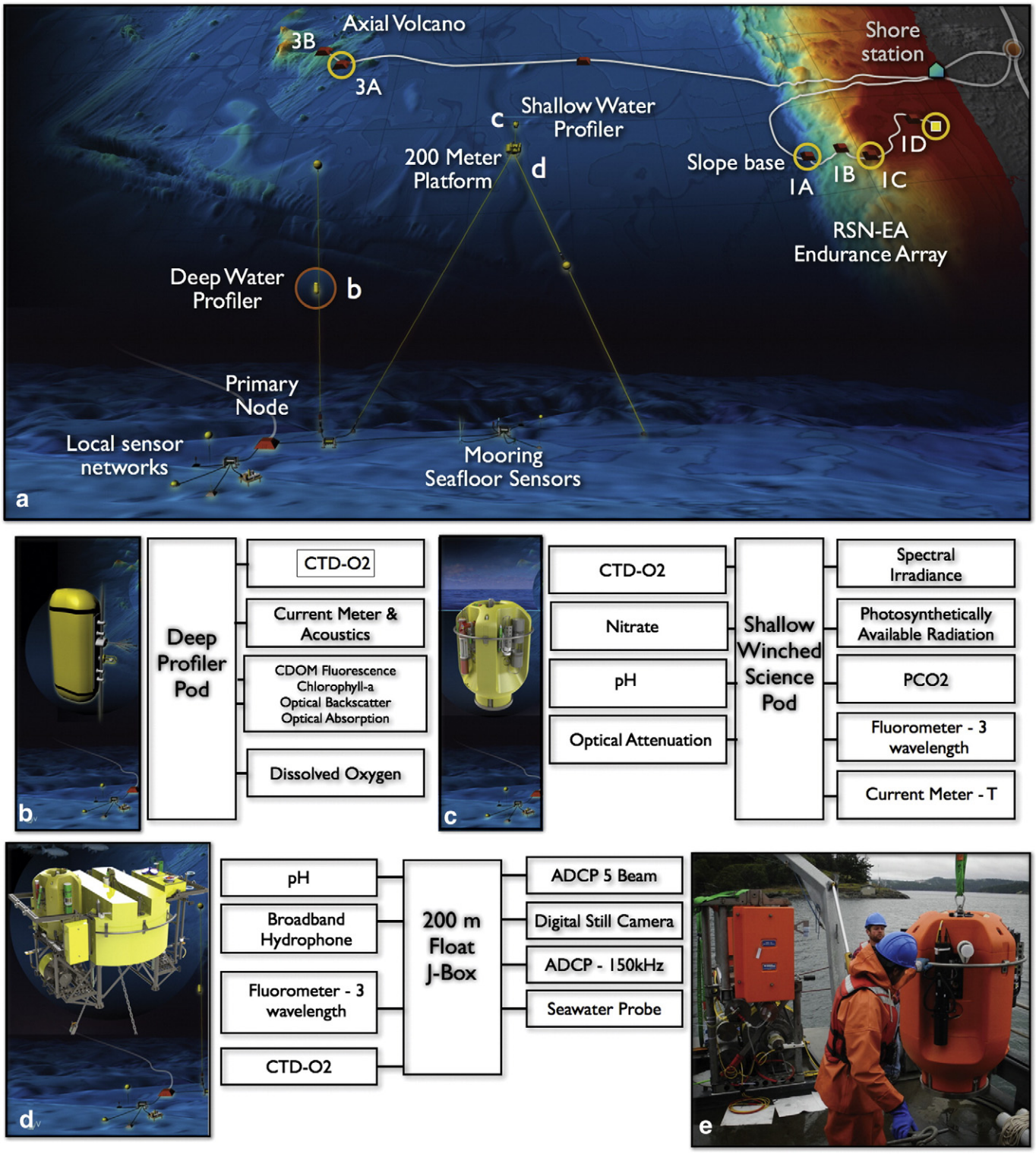

Fig. 7. a) The location of cabled moorings on the Regional Scale Nodes. These arrays will provide real-time measurement of physical, chemical, and biological parameters throughout the ocean depths. Sites 1A, 1C and 3A will included: 1) a Deep Profiler mooring; and 2) a two-legged mooring that will host an ~3.6 m-across instrumented platform and an instrumented Shallow Profiler; and 3) a seafloor node (not shown) that will include an upward-looking acoustic Doppler current profiler (ADCP), broadband hydrophone, optical attenuation sensor, CTD and dissolved oxygen (O_2), and an HPIES package that measures the horizontal electrical field that is proportional to the vertical averaged ocean velocity, an inverted echo sounder, and bottom pressure sensors (b). The Deep Profiler hosts an instrumented deep wire McLane profiler that will measure ocean properties from ~2800 m to ~200 m water depth. The profilers have been used at numerous locations in the oceans, but this one is modified so that power and data transfer will be provided via an inductive couple for year-long measurements. An extension cable running from a Low Power Junction Box will provide 375 V power and 1 Gbs communications. c) A model of a winched Shallow Profiler and associated instruments that will traverse from 200 m to just below the ocean's surface at least nine times a day. d) A science module (pod) on the 200-m platform and associated instruments is designed to be installed and recovered using a robotic vehicle. e) A Shallow Profiler being tested in winter 2014, for a follow-on summer deployment.

Table 2
Instrumentation at Axial and Endeavour.

	Axial[a]	Endeavour[b]	Measurements
Broadband seismometer with accelerometer	X	X	Global large magnitude earthquakes, melt migration, tremor
Short-period seismometers	X	X	Local earthquakes, melt and fluid migration, whale calls
Low frequency hydrophone	X		Acoustic tertiary waves of earthquakes
Bottom pressure sensor	X	X	Tides, storms, tsunamis
Current meter	X	X	Local currents
Bottom pressure — tilt instrument	X		Deflation and inflation of seafloor
Remote access fluid sampler	X	X	Chemistry of diffuse flow
Osmo fluid sampler	X		Chemistry of diffuse flow
DNA sampler	X		Microbial DNA, community structure
Temperature–resistivity–H_2	X	X	Black smoker fluid temperature, chlorinity, and hydrogen to monitor boiling, fluid–rock reactions
Temperature–pH–H_2S–H_2	X		Black smoker fluid temperature, acidity, hydrogen sulfide, and hydrogen concentrations to monitor boiling and changes in the reaction zone
Temperature–thermistor array	X	X	3D and linear temperature distribution in diffuse flow site
Mass spectrometer	X		Dissolved gas concentrations (e.g. carbon dioxide, methane, hydrogen sulfide) in diffuse flow
Digital still camera	X		Diffuse flow and black smoker sites — macrofauna and microbial distribution, changes in flow, smoker growth
High definition camera	X	X	Diffuse flow and black smoker sites — macrofauna and microbial distribution and changes in flow, smoker growth
Acoustic Doppler current profiler	X	X	Larger scale current velocities than current meter
Plume imager (COVIS)		X	Hydrothermal plume fluctuations combined with temperature measurements provide heat flux calculations
CTD	X	X	Conductivity, temperature, depth, ±dissolved oxygen of seawater and plumes

[a] See Figs. 7 and 10 for locations and number of each instrument installed at Axial in 2014.
[b] See Fig. 18 for locations and number of each instrument already installed at the Endeavour Segment or that are planned to be installed.

morphology, magmatic, tectonic, and seismic activity and in hydrothermal vent intensity and distribution (Fig. 3; Table 1). Because of these differences, these two systems provide optimal submarine observatory sites to quantify, and compare and contrast the evolution of geological, chemical, and biological processes along a MOR with the same spreading rate, but with very different magma budgets and tectonic activities. Both areas have a 2–3 decade history of observations through efforts that include the NSF RIDGE, CanRidge and NOAA Vents programs, which provided a strong foundation for the design and location of the cabled infrastructure at these two volcanoes.

Table 1
Axial Volcano and the Endeavour Segment characteristics.

	Axial	Endeavour
Spreading rate	~6 cm/yr	~6 cm/yr
Segment length	~100 km Axial Segment	~90 km Endeavour Segment
Topography	~1400 m of vertical relief, ~3 × 9 km caldera on summit with 100 m walls; ~50 km long rift zones to the north and south; associated with Cobb Hotspot.	Narrow, elongate volcano dissected by central rift ~100–150 m deep, 0.8–1.4 km wide rift valley dominated by a series of ridge parallel 1/2 ridges to the east and west.
Axial magma chamber	Long-lived large magma reservoir, greatest melt accumulated 2.5–3.5 km beneath caldera, dramatic changes in seafloor associated with eruptive events, very high CO_2 concentrations in melts.	Axial magma chamber underlies all hydrothermal fields extending ~25 km along axis at depths of 2.1 to 3.3 km beneath seafloor, 0.4–1.2 km wide, dips from north to south, distinct reflectors indicate discrete chambers.
Seismicity	1998 eruption marked by >8000 earthquakes lasting 11 days, 2011 eruption punctuated by 3.0 and 3.7 magnitude earthquakes, smaller quakes not measured due to SOSOS disrepair state; hydrophones in caldera recorded >1000 earthquakes/day.	Was highly seismically active until 2007, marked by 1000 earthquakes/year e.g. 12,000 detected in 2003–2004 — small magnitude, swarms in 1999/2000 and 2005; earthquakes near axial magma chamber reflector.
Magmatic activity	Frequent eruptions; erupted in 1998 and 2011; sheet and pillow flows, with collapse zones common; 1998 flow extended 9.9 km in length with 3 m subsidence recorded in caldera; 2011 flow extended >2.5 km across, ~10 km in length; erupted from a series of discontinuous *en echelon* fissures, prominent anastomosing channel systems; collapse zones commonly host pillars, with some actively venting diffuse fluids.	No historical eruptions documented, but seismic swarms and magmatic CO_2 pulses interpreted to reflect diking events beginning in 1999 and ending in 2007; very hard to map individual flows — commonly truncated, collapse zones common though not as expansive as Axial; East of eastern flank, several km-across and long, low-relief plain characterized by lobate and sheet flows, with collapse zones common.
Faults	100 m deep caldera with ring fault, extensive fissure system on the northeast side of the caldera hosting past two eruptions, significant fissures at far north and south ends of the caldera.	Steep normal faults common bounding the east and west rift walls, central rift hosts major fields; >1 km in length, 10s of m throw common, highly tectonized.
Hydrothermal vents	Three main vent sites — CASM, ASHES, International District. Small fields and chimneys with most ≪10 m tall. Largest chimney El Guapo reaches ~16 m in height; some flanges; 10s of chimneys; numerous diffuse flow sites along the east fissure system and at the southern end of the caldera.	Five major fields; North to South — Sasquatch, Salty Dawg, High Rise, Main Endeavour, and Mothra, ~200 m to 600 m in length; chimneys reach up to 45 m in height, 50 m across; flanges common; extinct field ~500 m in length; exposed stockwork system south of Mothra; 100s of extinct and active chimneys.
Fluids	Boiling common, temperatures up to 350 °C, compositions range from l ow-chlorinity to high chlorinity fluids, gas-depleted and -enriched fluids; high CO_2 concentrations, generally metal poor.	Intense phase separation (boiling and condensation) common until ~2001; Temperature of 402 °C measured in 1984; very high CH_4 and NH_4^+ concentrations for bare rock system; interpreted to reflect breakdown of organics in buried sediments, fresh fluid and brines exiting high-temperature sites
Diffuse flow	Within main three fields, diffuse flow is less common than at Endeavour; diffuse flow sites common along inferred expression of southern boundary fault; some sites contain dense microbial mats (e.g. Bag City).	Extensive diffuse low sites (20 m × 50 m or more across), common as haloes around and within smoker complexes, and as distinct distal sites (e.g. Quebec); some areas host nascent black smokers (e.g. Clam Bed).
Animal communities	Subset of wider-spread northeast Pacific vent community. Fewer species may reflect frequent habitat disturbance by volcanism.	More diverse vent faunal community. Several species known only from this area. Very large overall faunal biomass exploiting extensive venting on sulfide structures and basalt-hosted diffuse flows.
Microbial communities	Greater than decade-long studies of microbes pre- and following seafloor eruptions, DNA analyses show that diffuse flow sites are microbial "islands".	One of highest temperature organisms on Earth cultured from sulfide sample in Mothra (121 °C).

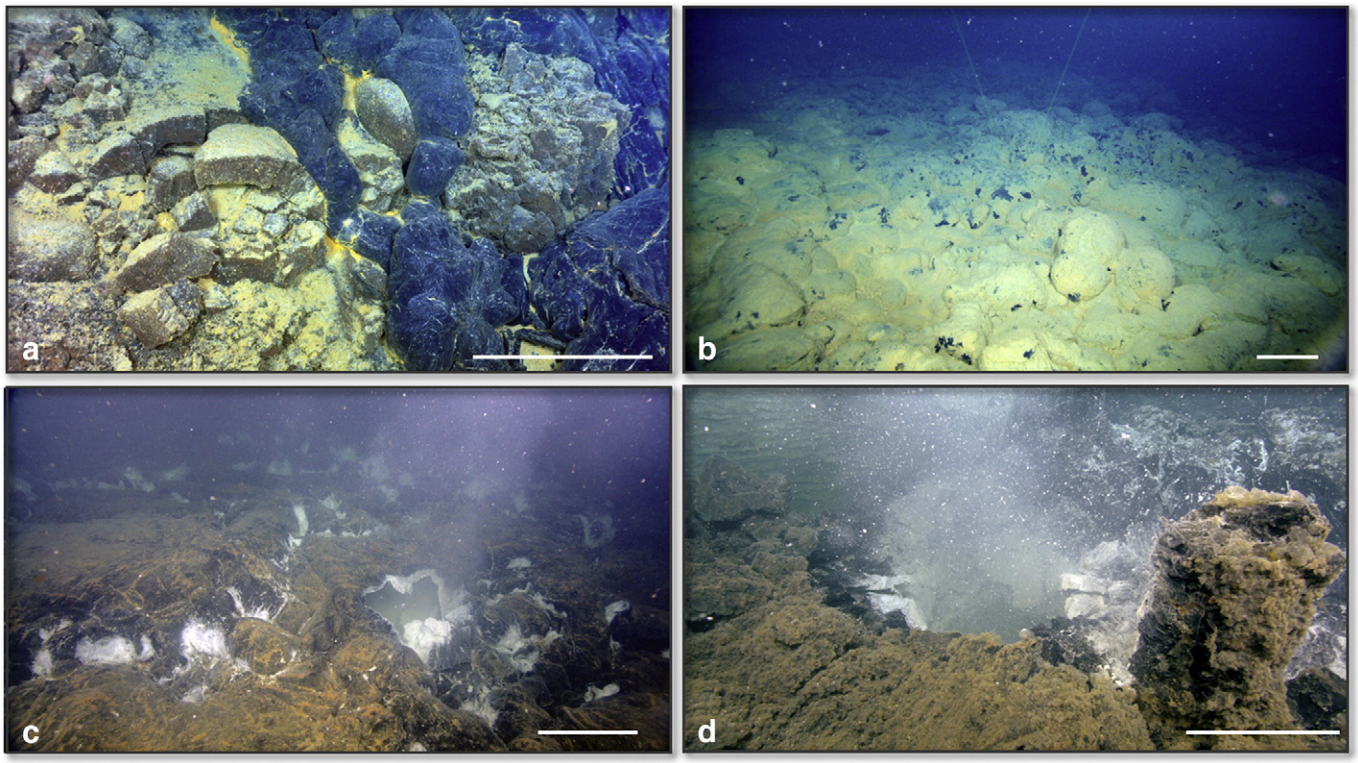

Fig. 8. a) Glassy lobate flow that cascaded down the eastern caldera wall in 2011. b) Three months after the April 6, 2011 eruption, pillow flows were covered with the remnants of yellow microbial mats. c) Snowblowers in the Skadi region emitting clouds of flocculant and microbial material. Skadi, in Norse mythology, is the goddess of winter and mountains. The skylights and crevices of the flows were lined with white microbial mats, while more distal regions were covered in brown mats. d) Close up of a skylight in the Skadi area showing flocculant material and bulbous growths of brown microbial mats on the outer surfaces of the collapse zone. Scale bar on all images is ~1 m across.
All images courtesy of OOI-NSF/UW/CSSF.

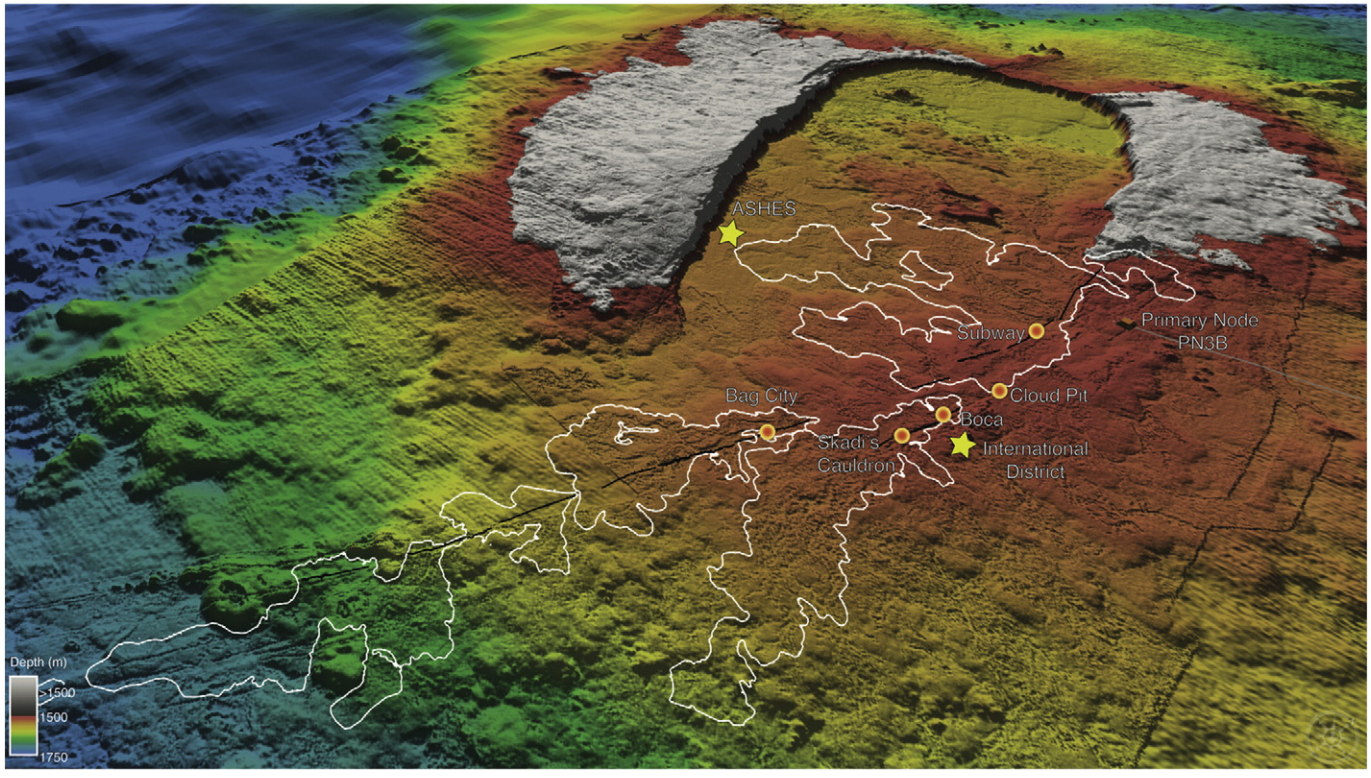

Fig. 9. Oblique view of the summit of Axial Seamount looking toward the northeast. In 2011, the landscape of the caldera was profoundly changed by a large eruption that extended ~3 km across the caldera (white line) and south along the rift system. Numerous snowblowers were produced as a result of the eruption (orange dots).

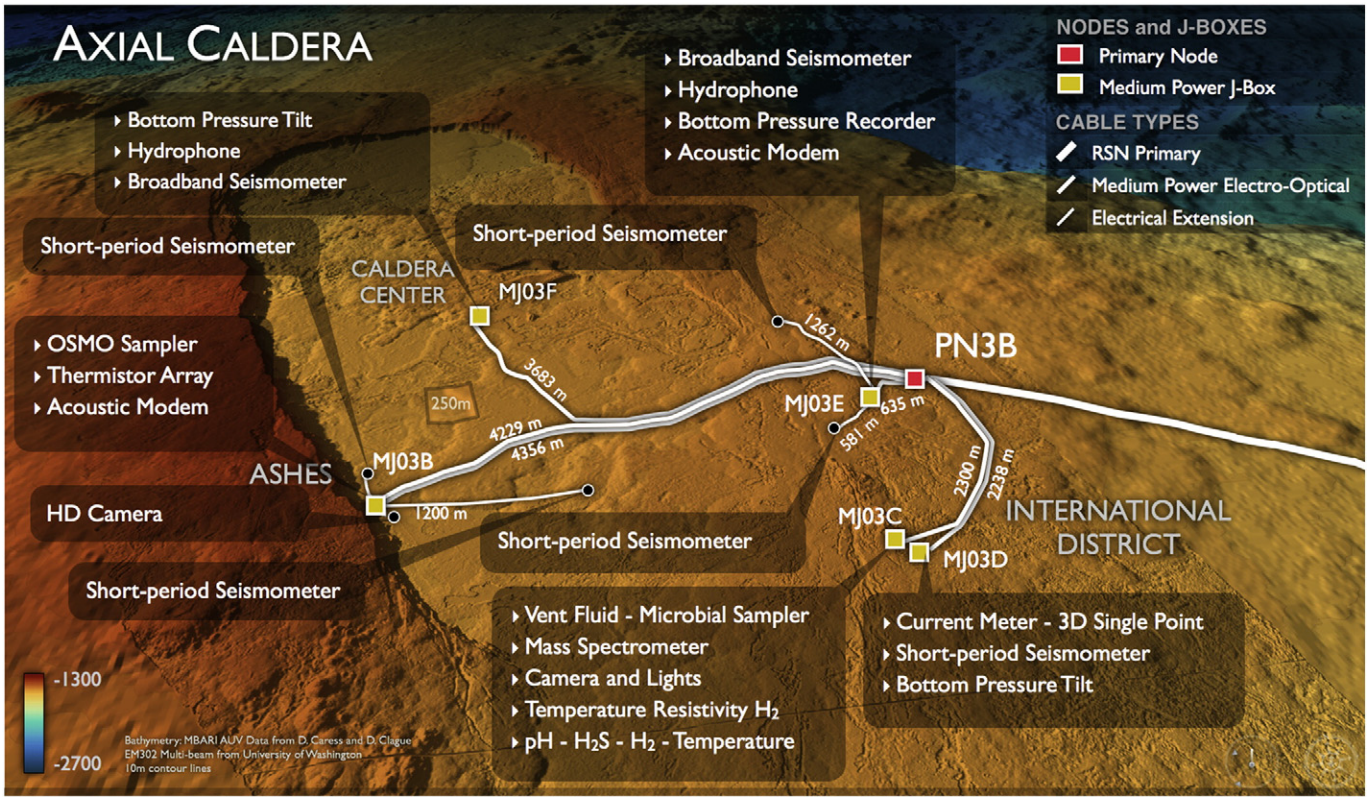

Fig. 10. Installed and planned cabled infrastructure at Axial Seamount. The primary backbone cable to Primary Node PN3B was installed in 2011. PN3B was installed and connected in 2012 and fully powered up. Medium power J-Boxes (e.g. MJ03B) provide power and communications to a diverse array of instruments. Also shown are the cable lengths for extension cables that connect J-Boxes to PN3B. All extension cables (~22,000 m) were installed and fully tested in 2013 using the *ROV ROPOS*. Installation of this entire array will be completed in summer 2014.

3.1. Axial Seamount

Axial Seamount, located ~500 km off the Oregon coast, is the most magmatically robust volcano on an ~500 km-long Juan de Fuca Ridge (Fig. 2). It dominates the morphology of the ridge, rising 1400 m above the surrounding abyssal plain and it is the youngest of a series of seamounts influenced by the Cobb–Eickelberg hotspot (Figs. 2 and 3) (Delaney et al., 1981; Embley et al., 1990; Chadwick et al., 2005). Its large topographic presence means that it impacts deep ocean currents around the volcano with mean flow circles that are anticyclonic (Lavelle et al., 2003). Seismic experiments show that there is a significant magma reservoir beneath the volcano, with the highest melt concentrations occurring at depths of 2.5–3.5 km (West et al., 2001). It is one of the best-studied volcanoes along the global MOR spreading system. It was the site of NOAA's NeMO (New Millennium Observatory) seafloor observatory and has been visited nearly annually for two decades. NEMO included an uncabled mooring, a few sensors, and very low bandwidth communications. It is the only submarine site where long-term measurements of summit inflation/deflation have been made prior to and following seafloor eruptions with implication for forecasting of Axial's next eruption (Chadwick et al., 1999; Nooner and Chadwick, 2009; Chadwick et al., 2012, 2013).

The summit of the volcano, at ~1500 m water depth, is marked by a horseshoe-shaped caldera that is 3.3 km across and 8.6 km in length (Chadwick et al., 2005; Clague et al., 2013). The caldera is bounded to the north and south by major, ~50 km long rift zones that are oriented ~15° to the spreading direction (Fig. 3) (Embley et al., 1990). The caldera walls are defined by near vertical, 100-m tall cliffs of truncated basaltic flows, marking a set of boundary faults that presumably dip inward toward the center of the caldera (Butterfield et al., 1990). The eastern side of the caldera is highly fissured with extensive collapse zones, sheet flows, and lava channels. In contrast, the southwestern side of the valley floor is paved over by lobate flows, and pillow flows that denote the edges of past eruptions. Numerous small pillow mounts and larger volcanic edifices, and massive pillow and lobate flows dominate the flanks of the volcano. Basaltic melts feeding the volcano have some of the highest dissolved CO_2 concentrations (9160 ppm) of any MOR volcano. These high values are consistent with widespread ash deposits up to 2 m thick on the volcanic flanks, which provide evidence for explosive volcanism (Helo et al., 2011). They are also reflected in the high CO_2 concentrations in both vent fluids and plumes (Butterfield et al., 1990; Resing et al., 2004).

3.1.1. Axial eruptions

Axial Seamount is one of only a handful of sites in the global ocean where historical seafloor eruptions have been visited shortly after or during the events (Haymon et al., 1991; Delaney et al., 1998; Embley, 1999; Fornari et al., 2004; Embley et al., 2006; Caress et al., 2012; Chadwick et al., 2013; Clague et al., 2013): Axial erupted in 1998 and again in 2011 (Embley, 1999; Lupton et al., 1999; Embley et al., 2000; Fox et al., 2001; Butterfield et al., 2004; Caress et al., 2012; Chadwick et al., 2012; Dziak et al., 2012; Chadwick et al., 2013). The 1998 eruption was punctuated by an intense seismic swarm, which within 6 h of initiation, migrated down the southern rift system. By the end of the second day it had reached 50 km to the end of the southern rift zone, with migration rates of ~0.9–0.2 m/s (Dziak and Fox, 1999). The seismic swarms, which were detected by the US Navy's Sound Surveillance System (SOSUS) hydrophone array, lasted 11 days with 8247 earthquakes detected (Dziak and Fox, 1999). The nature of the seismicity was similar to that observed during Icelandic and Hawaiian diking events (Einarsson and Brandsdottir, 1985; Rubin and Gillard, 1998). Based on depth differences between pre- and post-multibeam

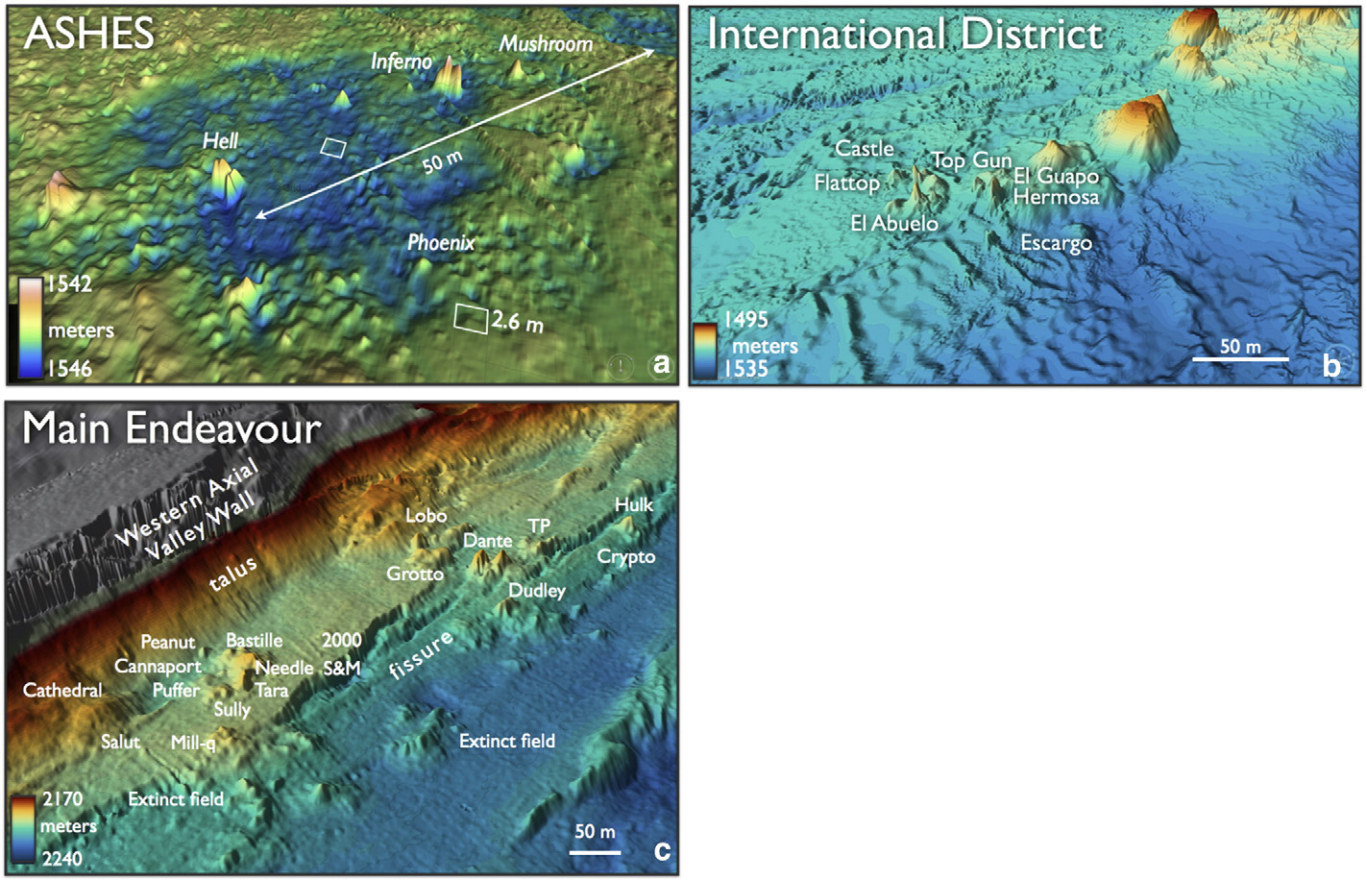

Fig. 11. Oblique views of hydrothermal fields at Axial Seamount and the Endeavour Segment. a) Meter resolution bathymetry of the ASHES hydrothermal field near the western caldera wall of Axial Seamount. These data were collected with the *ROV Jason* (Woods Hole Oceanographic Institution) using a RESON Seabat 7125 sonar system. The field hosts several small chimneys (Mushroom is ~4 m tall — see Fig. 15. b) The International District, located near the eastern fissure system, hosts the largest chimney at Axial, called El Guapo, which rises 16 m above the surrounding seafloor (see Fig. 14). The area is rugged, marked by extinct chimney debris, and hackly to lobate flows. c) The Main Endeavour Field on the Endeavour Segment was the most robustly venting hydrothermal field for >15 years. It is at a water depth of about 2200 m and hosts numerous black smoker chimneys that reach up to 50 m across and ~30 m high. The field is located on a 020 trending fissure system and is bounded to the west by the western rift valley wall. The area hosting the Bastille structure (known as the Bastille complex) is now waning in response to the 1999–2000 diking event. An extinct field marked by massive deposits of oxidized sulfide is located ~100 m east of the present day field and extends for >500 m along axis. The 5-m resolution bathymetry was collected in 2005 with the autonomous vehicle *ABE* using a Reson 2000 sonar.

bathymetric surveys, the eruption issued from the crest of the caldera fissure system and reached 9 km in length with an estimated volume of 18–76 $\times 10^6$ m^3 (Delaney et al., 2000). The eruption included four separate flows that issued from 11 eruptive fissures; a northern flow contained 70% of the erupted volume (Chadwick et al., 2013). The flows partially buried or covered mature hydrothermal vent communities, and resulted in the formation of new vent colonies (Embley and Baker, 1999). Three months after the eruption, new vents were colonized by tubeworms (*Ridgeia piscesae*) and by 30 months post-eruption, >60% of the vent-endemic species had colonized the new vents (Marcus et al., 2009).

Hydrothermal discharge was an order of magnitude greater than before the eruption, and hydrothermal plumes 200 m above the seafloor were enriched in methane (600 nM) and hydrogen (200 nM), and they contained high microbial abundances (Delaney et al., 1998; Cowen et al., 1999; McLaughlin-West et al., 1999). The steady-state heat flux required to produce a plume found 20 km distal to the eruption was estimated to be 60–230 GW (Baker et al., 1999). This was one of the first sites where snowblowers were well documented with floc and milky white fluid issuing from skylights in lobate flows and along fracture systems (Butterfield et al., 2004; Chadwick et al., 2013). Small fissures were completely coated with white microbial mats. Most of these sites were highly ephemeral, but one vent called Cloud that issued intense smoky fluid in 1998, was still active 18 months after the eruption, although flow had decreased and the fluids had turned milky in appearance (Butterfield et al., 2004; Chadwick et al., 2013). Flows that were thicker than ~2 m were covered with white to tan colored microbial mats. Degradation and the eventual disappearance of the mats occurred a few years post-eruption (Chadwick et al., 2013).

On April 6, 2011, the summit of Axial Seamount was again significantly transformed by an eruption with flows reaching nearly 3 km across the floor of the caldera, and at least 10 km in length along the eastern fissure zone (Figs. 8 and 9) (Caress et al., 2012; Chadwick et al., 2012). The eruption was not detected by the SOSUS array because it was functioning poorly. Therefore, the eruption was not discovered until a NOAA dive program in July 2011. The NOAA expedition directly imaged the new flow with documentation of several long-term monitoring sites buried by up to 4 m of new lava (Fig. 8) (Chadwick et al., 2012). During the course of the summer, three field programs using the robotic vehicles (ROVs) *Jason*, *Doc Ricketts*, and *ROPOS* [NOAA, MBARI (Monterey Bay Aquarium Research Institute), and UW-led, respectively] made direct observations of the flow and resultant hydrothermal activity, and sampled the eruption and associated plumes. Within a week of NOAA's discovery of the eruption, MBARI's autonomous underwater vehicle, the *D. Allan B.*, mapped the flows in and near to the caldera to 1 m resolution (Caress et al., 2012). Following this, the entire extent of the eruption was mapped by the EM302 system on the *R/V Thompson* during the UW-OOI expedition (Fig. 9) (Caress et al., 2012).

Several years of bottom pressure measurements following the 1998 eruption showed that the rate of inflation increased in the months leading up to the 2011 eruption (Chadwick et al., 2012), with an average rate of ~16 cm/yr from 2007 to 2010. This rate increased to 34 cm/yr

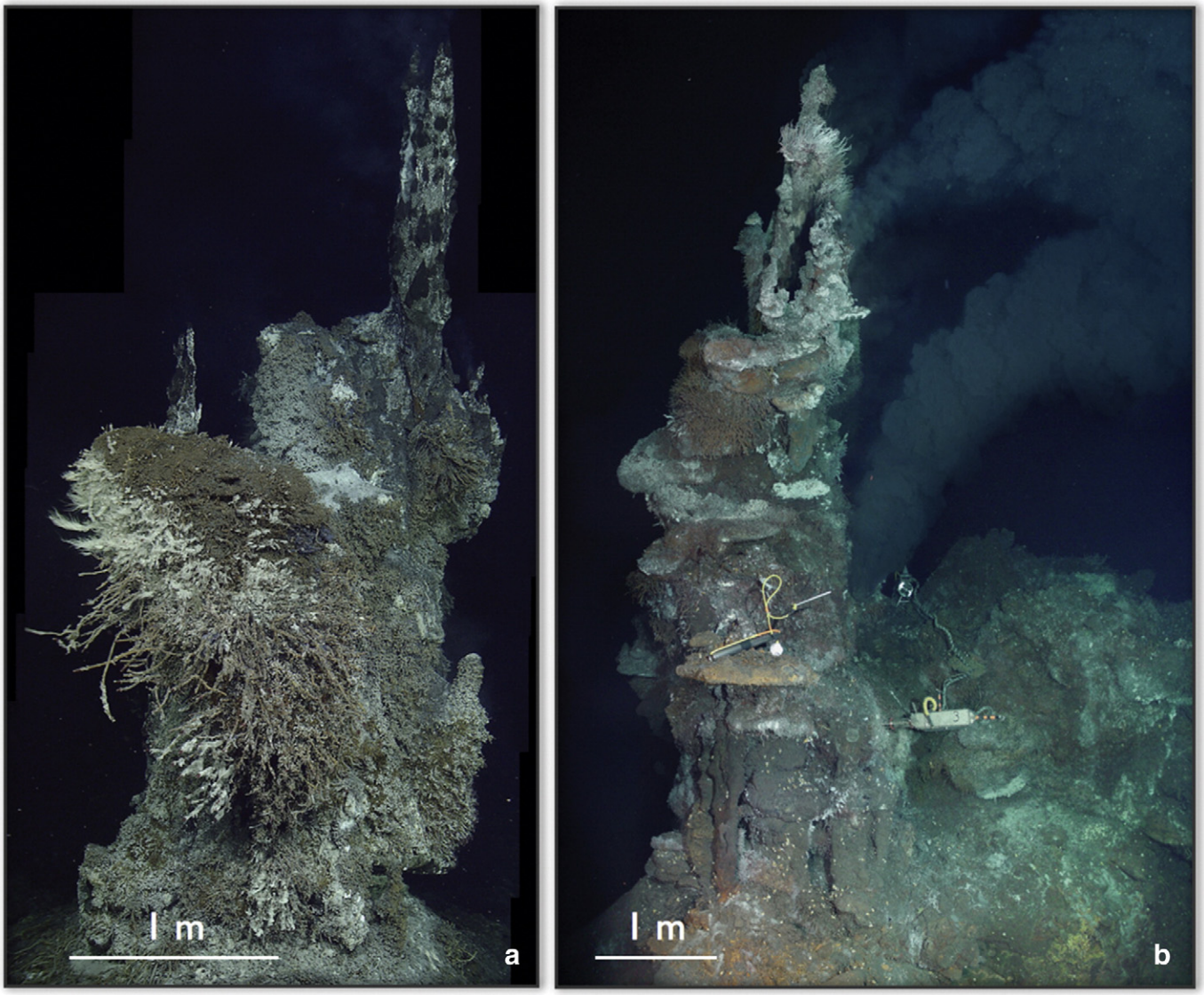

Fig. 12. a) The black smoker chimney 'Inferno' rises ~4 m above the seafloor in the ASHES hydrothermal field. A young, friable chimney caps the top of the edifice and emits relatively particle-poor fluids. Dense assemblages of limpets, tubeworms, palm worms and scale worms cover much of the structure. b) The black smoker edifice 'Milli-q' in the Main Endeavour Field was venting 360 °C fluids in 2003. This multiflanged structure in 2003 hosted numerous active and extinct ledges, or flanges whose underbellies host reflective pools of high-temperature hydrothermal fluids. A microbial incubator designed to examine the upper temperature limit of life in the walls of black smoker chimneys is inserted into an experimental hole in the side of the edifice. A data logger in the background measured temperatures every 20 min on 12 temperature probes for the year 2003–2004. In contrast to the chimneys at ASHES, the edifices at Main Endeavour emit dense "smokey" plumes of fine-grained sulfide. Milli-q is now extinct.
These two photomosaics were produced by M. Elend, University of Washington.

from 2010 to the eruption, and to 50 cm/yr from January to March, 2011. Over the 2010 period, there was a concomitant increase in the number of seismic swarms. On April 6 and 7, 3.0 and 3.7 magnitude earthquakes were recorded, respectively, by land-based stations. In April 6, earthquakes recorded by ocean bottom hydrophones within the caldera had increased to >1000/day (Dziak et al., 2012). That same day, there was a drastic change in inflation rates of the caldera floor with 7 cm to 13 cm of uplift occurring in 40 to 55 min. This was followed by rapid deflation that lasted 6 days and resulted in 2.4 m of subsidence in the center of the caldera (Chadwick et al., 2012). These data are consistent with an eruption beginning in April 6 (Chadwick et al., 2012; Dziak et al., 2012). The eruption included flows issuing from fissures just outside of the caldera, which in the north resulted in glassy flows that cascaded down the caldera walls (Figs. 8 and 9). The toes of the flows, composed predominantly of pillow basalts, are the thickest parts of the flows (reaching 17 m in thickness), and they are also where the most massive microbial mats formed immediately following the eruption (Fig. 8b) (Caress et al., 2012 and Chadwick et al., 2012). It is estimated that the 2011 eruption resulted in ~147×10^6 m^3 of magma being removed from the summit reservoir (Chadwick et al., 2012).

One of the most impressive consequences of the eruption was the development of numerous, spectacular snowblowers that formed along the eastern rift system, but which were also present at the southern termination of the caldera (Figs. 8 and 9; e.g., Bag City). Most of the snowblowers were sourced in collapse pits that reached several meters across and a few meters deep. Others issued from small skylights in lobate flows and from the interstices between lobate flows (Fig. 8c and d). Thick, white microbial mats coated the entire surfaces of the collapse zones and individual lava pillars. Significant egress of methane-rich diffuse fluids issued from the subsurface, forming dense clouds. The fluids were just above ambient temperature and contained massive amounts of flocculant and microbial material (Fig. 8c and d) (Proskurowski et al., 2012; Meyer et al., 2013). Chemical gradients around the collapse zones resulted in zoning of microbial

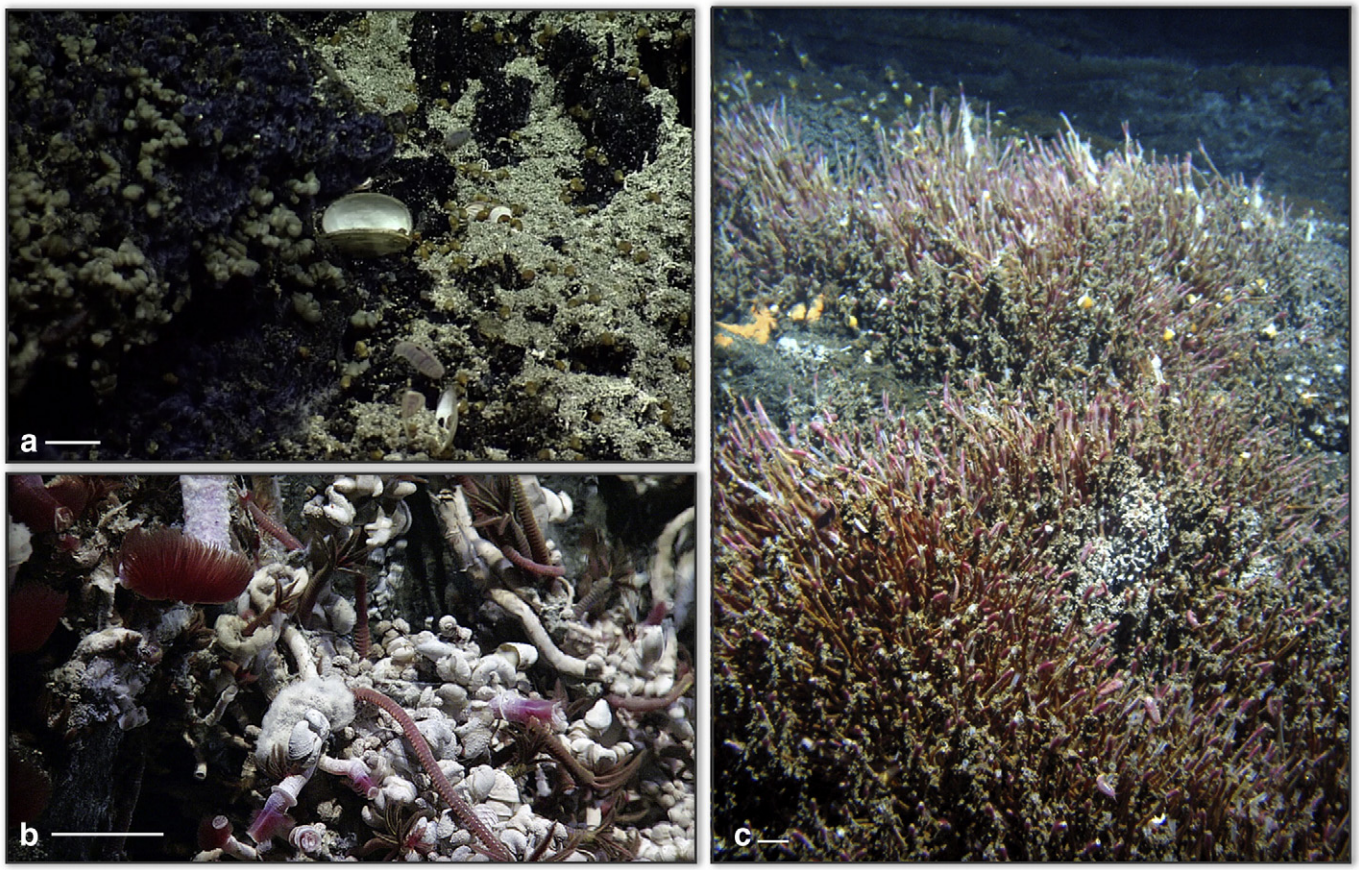

Fig. 13. a) Macrofaunal communities in a diffuse flow area at the base of the venting structure 'Escargo' in the International District hydrothermal field. One key characteristic of Axial faunal communities is the presence of clams (which are rare at Endeavour, except for at the Clam Bed site). Also shown are blue ciliates and limpets (left portion of image), gastropods, and abundant Pycnogonadea (sea spiders). b) Dense colonies of tubeworms hosting bright red plumes, and palm and sulfide worms thrive in warm fluids issuing from the side of the 305 °C smoker called 'Finn' in the Mothra hydrothermal field on the Endeavour Segment. A scale worm (central left portion of image) is coated by filamentous bacteria. These carnivorous animals feed on the plumes of tubeworms. Very high concentrations of limpets commonly coat the outer walls of the chimneys. c) Several tens of meters across diffuse flow site bound the base of a 50 m-across, actively venting sulfide structure called 'Hulk' in the Main Endeavour Field. Here, diffuse flow issues from cracks in a sheet flow, supporting rich assemblages of skinny tubeworms, scale worms, and limpets. Yellow snails and orange bacterial mats are present in areas of weaker diffuse flow.

community structure: white mats dominated areas of most intense flow while brown-orange mats where abundant on the surfaces of adjacent basaltic flows (Fig. 8c and d). Analyses of the V6 region of 16S rRNA and quantitative PCR show that the white flocculant/microbial mats were dominated by *Epsilonproteobacteria*, while the orange floc was dominated by *Gammaproteobacteria*, with only 1% of the community DNA belonging to archaea (Meyer et al., 2013). The white floc was dominated by elemental sulfur that likely resulted from sulfide-oxidizing organisms. The issuing fluids and white floc also contained Methanococcales and anaerobic thermophilic archael groups, requiring that these organisms were sourced from the subsurface (Meyer et al., 2013). The orange mats contained iron-oxidizing bacteria, and lower concentrations of sulfur-oxidizing bacteria than the snow blowers, as well as organisms that colonized on settled plume particles, and multicellular debris (Meyer et al., 2013). The massive ejection of fluids from beneath the seafloor and from the lava flows resulted in cloudy water that filled much of the caldera, leading to much poorer visibility than normal (Fig. 8c). The snowblowers may serve as important seeding sites for follow-on microbial and macrofaunal systems (Juniper et al., 1994).

The past two eruptive events at Axial Seamount show that it is a highly dynamic system marked by significant inflation and deflation events and intense seismic activity. To monitor precursor, eruption and posteruptive behavior of the volcano, the RSN includes an array of bottom-pressure tilt instruments, short-period and broadband seismometers, and low frequency hydrophones distributed within and adjacent to the caldera (Fig. 10). Over 22,000 m of secondary extension cables were installed in 2014, as well as two secondary nodes, and five short-period seismometers (Fig. 10). During an 11-h testing event using the *ROV ROPOS* to power up the secondary nodes, cables and seismometers, 15 earthquakes were detected below the summit of the volcano. When fully installed and connected in 2014, these instruments will provide real-time data on melt migration within the volcano, inflation and deflation, and seismic activity associated with eruptive events. The seismic data will be integrated into NSF's funded IRIS (Incorporated Research Institutions For Seismology) database. This is the first submarine volcano to host such an array of instruments.

No megaplume was detected at Axial, probably because the volcano was not visited until three months after the eruption. However, the moorings at the base of Axial Seamount (2700 m) may allow characterization of megaplumes in follow-on eruptions (Figs. 2 and 7). The moorings include an instrumented wire crawler that goes from 2700 m water depth to ~600 m (Fig. 7). A second, two-legged mooring includes an ~3.6 m-across instrumented platform hosting, for example, a digital still camera, acoustic Doppler current profiler, broadband hydrophone, and fluorometer. The platform also includes an advanced winched profiler (with an underwater level wind), which measures ocean parameters from 600 m to just below the surface (Fig. 7c and d). At least nine profiles will be completed each day. Two-way

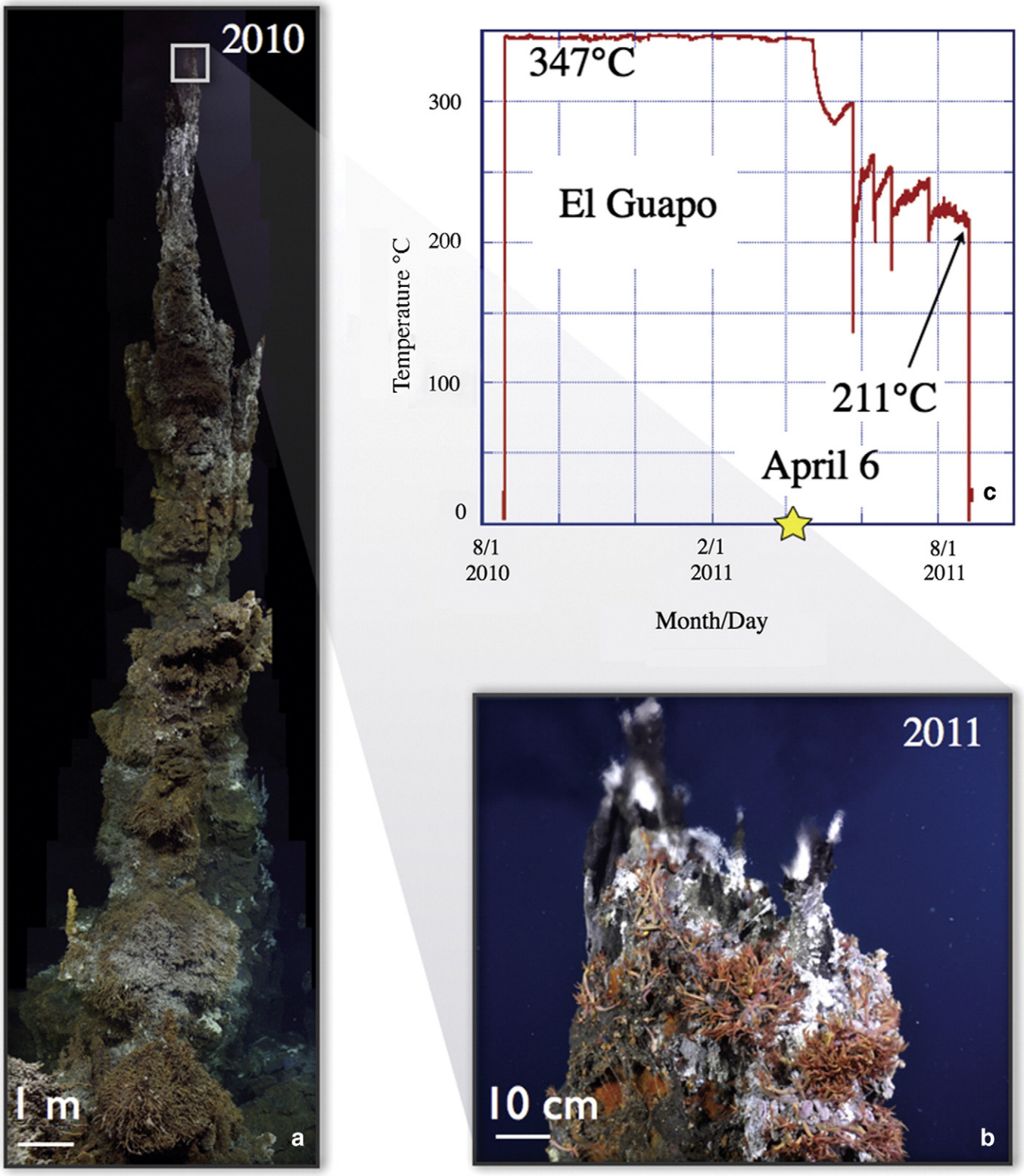

Fig. 14. a) Photomosaic of an ~16 m tall black smoker edifice called El Guapo in the International District hydrothermal field. For several years, this structure issued (~350 °C) boiling fluids from small spigots at its summit (b). b) Small orifices emit clear end-member hydrothermal fluids, which rapidly entrain seawater, resulting in precipitation of fine-grained sulfide. Healthy patches of palm and sulfide worms cluster near the summit of El Guapo. c) Temperatures of El Guapo in 2010–2011 measured with a HOBO sensor placed directly inside one of the orifices at the summit of the edifice. For several months prior to the April 6 eruption, vent fluid temperatures showed little variation from the 347 °C venting temperatures. However, several days after the eruption, temperatures dropped precipitously, reaching 211 °C when the probe was recovered on August 1, 2011. The HOBO was still deep within the throat of the venting spigot, so these temperature drops do not reflect movement of the sensor to outside of the orifice.

communication allows response capabilities that would include, for example, stopping at a plume anomaly to measure particulate concentrations, conductivity and dissolved oxygen, pH, and the partial pressure of CO_2.

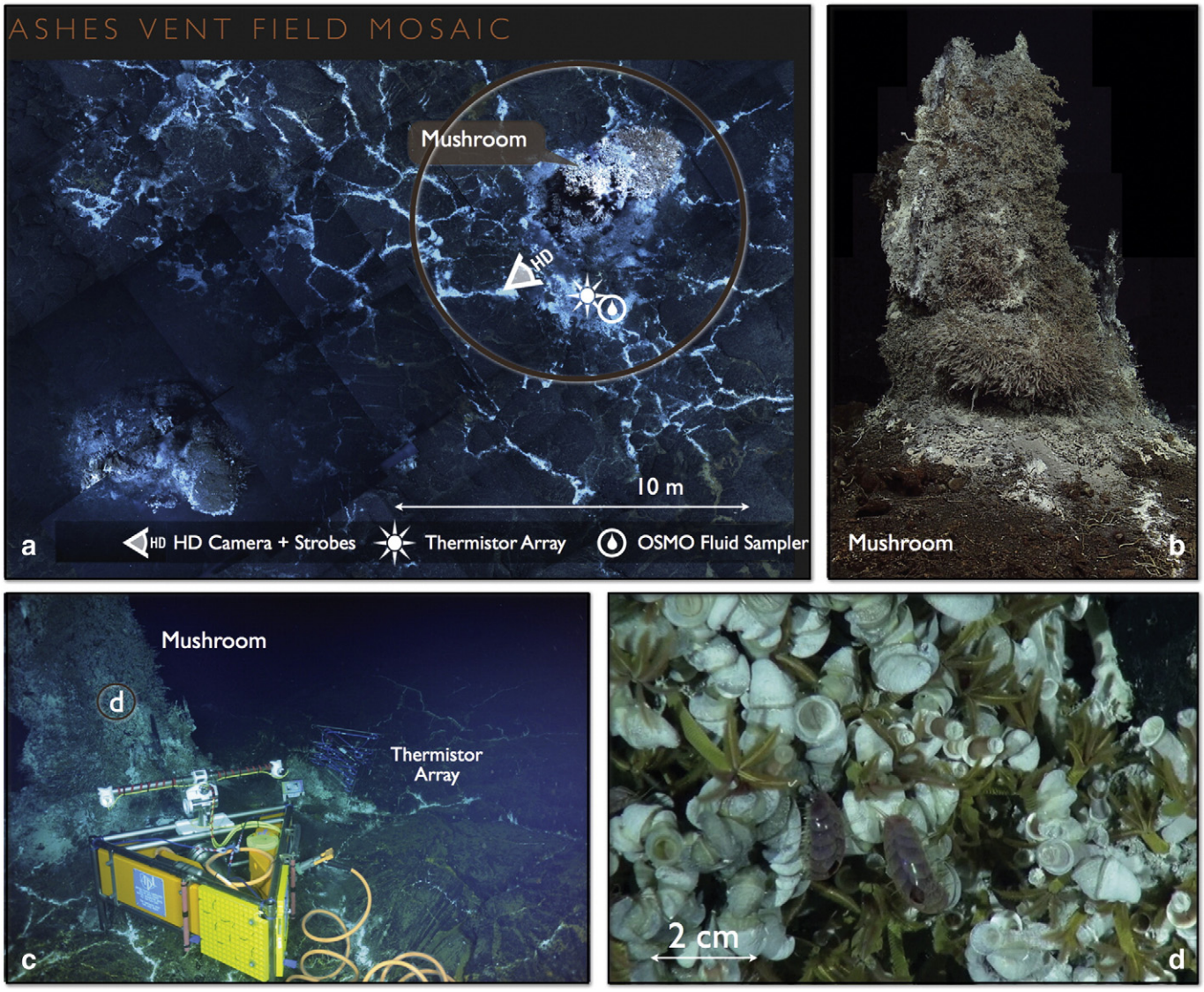

Fig. 15. a) Down-looking photomosaic of a portion of the ASHES hydrothermal field in 2010 using the *ROV Jason* and the active hydrothermal chimneys 'Mushroom' and 'Inferno' (bottom left corner). The entire mosaic includes 6000 images. White cracks radiating from Mushroom are sites of diffuse flow and host microbial communities, tubeworms and clams. Also shown is the site where the high definition (HD) camera and thermistor array were installed in 2013. b) A photomosaic of an ~4 m-tall chimney Mushroom. c) A cabled high definition camera installed near the southwest face of Mushroom. In 2014, it was fully tested along an ~4 km of extension cable using the *ROV ROPOS* for power and communications. It will be connected to Primary Node PN3B, summer 2014 and commence streaming live video. d) A framegrab of the live video was streamed from the camera onto the Internet in 2013 during the VISIONS'13 expedition (http://interactiveoceans.washington.edu/story/VISIONS_13). This area is covered in white limpets, red scale worms and brown-orange palm worms.
a) Photomosaic by M. Elend, University of Washington.

3.1.2. Hydrothermal fields

The central caldera hosts three main hydrothermal fields, CASM (Canadian American Seamount Expedition), ASHES (Axial Seamount Hydrothermal Emissions Study), and the International District (Figs. 3, 9–15; Table 1). In addition to these fields, there are myriad diffuse flow sites with most located in an ~4 km zone along the eastern fissure system, and in the southern area of the caldera along the inferred boundary fault that is buried by lava flows (Butterfield et al., 1990, 2004; Clague et al., 2013). The southern area also hosts a few small and isolated actively venting chimneys. The three hydrothermal fields are small compared to many mid-ocean ridge sites — the individual fields host only a handful of chimneys each (Fig. 11a and b). The ASHES and International District Hydrothermal Fields were chosen as the key cabled instrumentation sites.

The main part of the ASHES field is located in a small, few meter deep depression that is ~60 m across and it hosts <10 structures (Fig. 11a) The International District is ~60 m across with <15 sites of active flow (Fig. 11b). The NOAA Vents program has intensely sampled many of the venting sites, particularly ASHES, the International District and the southern caldera (Massoth et al., 1989; Butterfield et al., 1990, 2004; Hammond, 1990). It is the only place where long-term, corresponding temperature, chemical, and microbiological analyses have been completed in numerous diffuse flow sites nearly annually for over a decade, prior to and following seafloor eruptive events (Huber et al., 2003, 2006, 2007; Butterfield et al., 2004; Opatkiewicz et al., 2009). A remarkable finding from these studies is that the diffuse flow sites, meters to kilometers apart, are persistent microbial 'islands', hosting distinct microbial populations that evolve over time, but which stay distinct even after an eruption (Opatkiewicz et al., 2009).

The ASHES vent field is located ~130 m east of the caldera boundary fault. The depression, with only a few meters of relief, is floored by fractured lobate flows and some sheet flows. Many of the narrow fractures are diffusely venting and support tubeworms, palm worms, limpets and rare clams (Fig. 15). The chimneys are generally small (less than ~4 m in height) (Fig. 11a) and typically host numerous very narrow discharge orifices (<5 cm). They are commonly covered

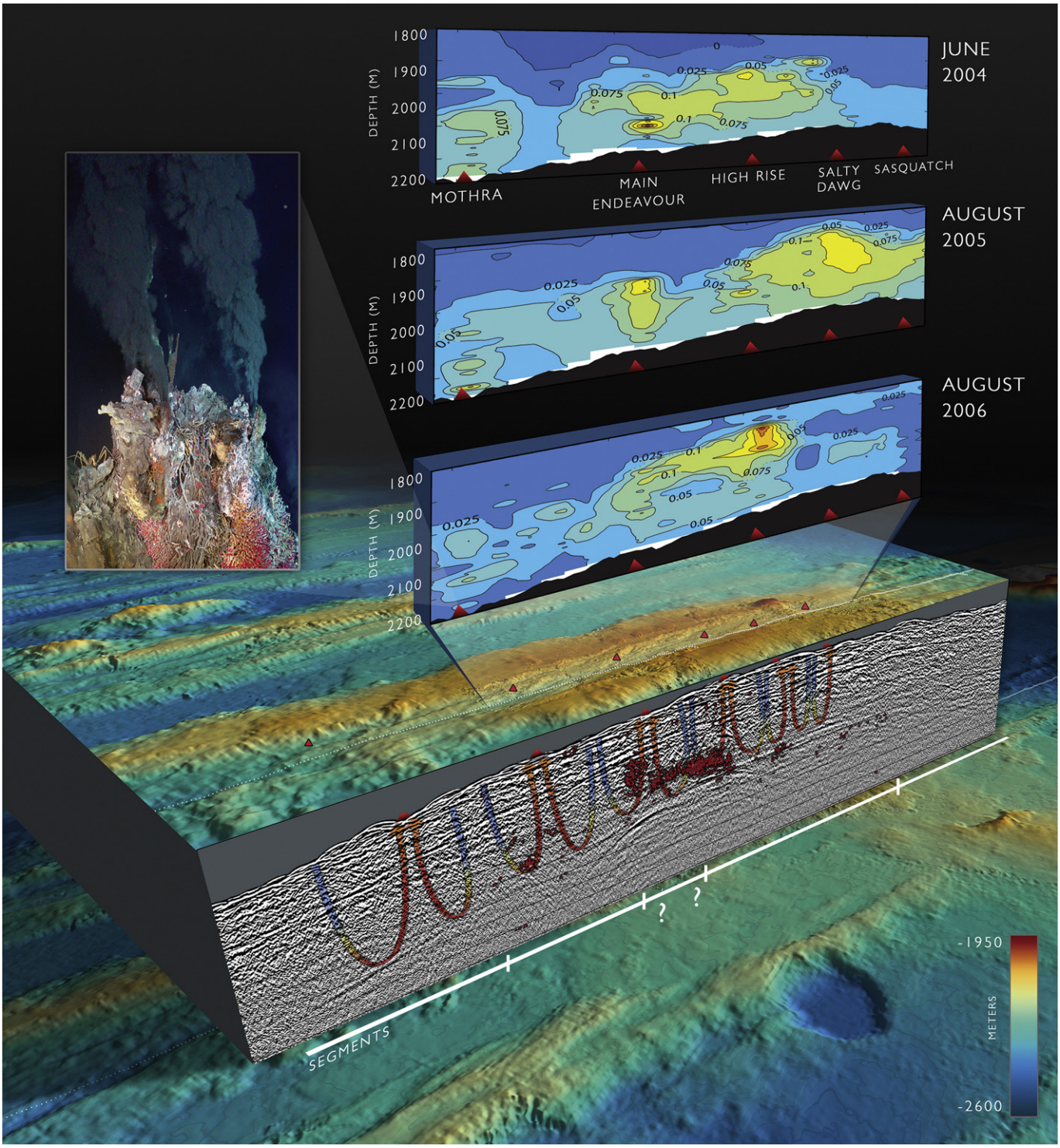

Fig. 16. Interdisciplinary lithosphere to hydrosphere representation of the Endeavour Segment. This image shows the surface bathymetry underlain by multichannel seismic results from Carbotte et al. (2012) and Van Ark et al. (2007). For ease in viewing and graphical representation, the along-axis transect has been moved slightly to the east of the ridge axis — the location of the along-axis survey line within the axial rift is indicated by a white dashed line. A magma chamber reflector is found beneath all five of the vigorously venting hydrothermal fields (red triangles), as well as beneath the newly discovered Stockwork system to the far south that is underlain by another strong reflector as defined by Van Ark et al. (2007). The magma chamber near the inflated, shallowest section of the ridge shoals to a depth of ~2.1 km beneath the seafloor and deepens significantly to the south to a depth of 3.3 km (Van Ark et al., 2007). Differences in the seismic reflection indicate that the magma chamber is composed of four sections. The red circles show the hypocenters for double-difference earthquake locations lying within 1 km of the location of the seismic profile (Wilcock et al., 2009). Also shown are inferred patterns of upflow and downflow (arrows) as first described by Delaney et al. (1997). The three panels projected above the spreading center show the objectively mapped potential temperature anomaly sections resulting from repeat hydrography surveys in the summers of 2004–2006 (Kellogg and McDuff, 2010). Historically, the Main Endeavour and High Rise hydrothermal fields have yielded the largest and most intense buoyant plumes, corresponding to the largest and most vigorously venting hydrothermal structures and the most intense seismic activity.

in dense macrofaunal communities that are similar to those at the diffuse flow sites, but they lack clams (Figs. 12a, and 15a and b). Many of the chimneys have remained similar in size since the late 1980s (Butterfield et al., 1990; Hammond, 1990). New growth forms slender, highly friable spires that are rich in anhydrite, pyrite and zinc sulfide. The venting fluids are relatively particle-poor

compared to many high-temperature chimneys (Butterfield et al., 1990). The northeastern portion of the field hosts a <1 m tall anhydrite spire (Virgin mound) bounded by a small anhydrite mound that vents clear fluids and emits some of the highest CO_2-rich fluids in the caldera (Butterfield et al., 1990).

Infrastructure at ASHES is focused on examining the relationships between seismic activity and fluid flow in diffuse and black smoker sites, and how changes in diffuse fluid temperature and chemistry impacts macrofaunal communities. A high definition video camera, long-duration fluid sampler, and a three-dimensional thermistor array are located at the chimney called Mushroom (Figs. 11 and 15). A tight array of three short-period seismometers feeding out from this site is designed to capture local seismic events beneath the field, with the goal of defining the nature of the upflow zone beneath ASHES (Fig. 10).

The International District is located on the southeastern fissure system just outboard from the southeastern boundary fault (Figs. 3 and 10). It is an area of rugged topography with lobate, pillow and sheet flows, and wide areas of hackly flows (Fig. 11b). The area is bounded to the west by expansive collapse zones and lava channels, and to the north by numerous 10s of meter-tall constructional highs. Extinct chimneys on the edges of the field are wrapped by lava flows that post-date chimney formation. The field hosts the tallest chimneys at Axial, with El Guapo (the handsome one) reaching ~16 m in height (Figs. 11b and 14). Also present within the field are abundant extinct sulfide deposits that include a 9-m tall chimney and significant sulfide talus and debris. Many of the chimneys host well developed flanges, reminiscent of those that characterize the Endeavour system. Hydrothermal activity is typically most intense near the tops of the chimneys and it is commonly marked by small, highly friable spigots. On El Guapo, these jet clear fluids that resemble underwater "fire"(Fig. 14b). Diffuse flow sites occur at the base of the chimneys and along steep sided slopes (e.g., near base of Escargo). These sites host dense patches of blue colonial ciliate mats, tube and palm worms, limpets, squat lobsters and abundant sea spiders (Pycnogonida) (Fig. 13a).

Historically, numerous chimneys within the Axial system have emitted boiling fluids that are high in magmatic CO_2 (>150 mmol/kg) (Butterfield et al., 1990, 2004), consistent with the high CO_2 concentrations of the basaltic melts (Helo et al., 2011). High-temperature fluids depleted in chloride, reflect boiling within this relatively shallow system (Butterfield et al., 1990) (Fig. 14). El Guapo was profoundly impacted by the 2011 eruption (Fig. 14). In 2010 and during the first three months of 2011, El Guapo was venting 347 °C boiling fluids. Shortly after the April eruption, vent temperatures had only dropped a few degrees. However, by May 11, 2011, temperatures were at 283 °C, and by August 1, when the temperature sensor was removed from inside the orifice, the vent fluid temperatures were 211 °C (Fig. 14c).

Numerous diffuse flow systems were particularly impacted by the past two eruptive events, resulting in the partial to full burial of some sites, production of nascent diffusely venting areas in others, and production of short-lived snowblowers (Butterfield et al., 2004). Some diffuse flow sites that predate the 2012 eruption are still active even though they were paved over with new lava. Detailed chemical analyses by Butterfield et al. (2004) show that the chemistry of the diffuse fluids is sourced in the high-temperature reaction zone (>350 °C), and over printed by lower temperature reactions that result in the production of methane, ammonia, and elemental sulfur.

Because the International District is the largest hydrothermal field and located near the eastern fissure network, it was chosen as the site to focus on both high- and low-temperature venting processes. Here, some of the most technologically advanced instrumentation is located, including a mass spectrometer to measure the volatile chemistry of diffuse fluids, adaptive diffuse fluid (major and trace element chemistry) and microbial DNA samplers, and two instruments to measure high-temperature vent fluid and volatile chemistry. These last two sensors will be placed within the throats of two high-temperature chimneys and will measure temperature, pH, H_2S, H_2, and resistivity (Figs. 6c and 10). A digital still camera will provide imaging at the same location as the mass spectrometer, and coupled diffuse fluid and microbial DNA sampler. A seismometer, bottom-pressure tilt instrument, and current meter are located nearby (Figs. 6 and 10).

3.2. Endeavour

The 90 km-long Endeavour Segment is part of a dueling propagator with the Cobb Segment to the south and the Middle/West Valley to the north (Fig. 2 and Table 1) (Karsten et al., 1986, 1990). The central third of the segment is a 25 km-long volcanic high split by a 75–200 m deep, 0.5–1 km wide steep-sided axial rift (Fig. 3b). This central rift hosts five major hydrothermal vent fields (from north to south — Sasquatch, Salty Dawg, High Rise, Main Endeavour, Mothra), more recently discovered smaller fields (Raven, Stockwork), and several distal, diffusely venting fields (Cirque, Dune, Clam Bed, Quebec) (Figs. 3b and 16). It is one of the most active hydrothermal areas known on the MOR system. The valley exhibits an hour-glass shape, becoming its narrowest immediately south of the Main Endeavour Field (MEF) and broadening to a width of ~3 km at the south end of the segment (Fig. 3b) (Delaney et al., 1992). The northern portion is marked by numerous horsts and dissected ridges that begin near the High Rise hydrothermal field and extend north of Summit Volcano.

Seismic studies show that magma bodies underlie all of the known hydrothermal fields (Fig. 16) (Van Ark et al., 2007; Carbotte et al., 2012). From north to south, the axial magma chamber deepens from 2.2 to 3.3 km beneath the seafloor, respectively (Van Ark et al., 2007; Carbotte et al., 2012). High Rise, Salty Dawg and Sasquatch are all within the central portion of the shallowest lens segment from 47°56.8′ to 48°00.5′N. The MEF is located above a zone of complex reflectivity at the southern end of this segment (Fig. 16). Hydrothermal flow is focused along normal faults, trending at ~020 within the axial rift and inner walls (Delaney et al., 1992; Kelley et al., 2001b, 2002; Glickson et al., 2007). Mothra, which is about 3 km south of the MEF, is underlain by a strong axial magma chamber reflector at about 2.5 km beneath the spreading axis (Van Ark et al., 2007).

3.2.1. Diking events

No historical seafloor eruptions have been detected on the Endeavour Segment, although it appears that from 1999 to 2006 there was a spreading-dike intrusion event(s) that impacted West Valley and the Endeavour Segment (Weekly et al., 2013) The 20-year SOSUS earthquake catalog (Dziak et al., 2011) shows that the Endeavour Segment lies in a region of elevated background seismicity, which likely results from the reorganization of plate boundaries in the region. The reorganization is due to the presence of an unstable triple junction at the northern end of the Juan de Fuca Ridge, which formed when the Explorer plate detached from the Juan de Fuca Plate along the Nootka transform fault (Fig. 2). In addition to the elevated background level of seismicity, Endeavour has been punctuated by three major seismic swarms during the last two decades.

Two elevated periods of seismic activity were recorded in June 1999, and January 2000 (Lilley et al., 2003; Bohnenstiehl et al., 2004), and another in February 2005 (Hooft et al., 2010). The 1999 activity lasted 5–11 days and spanned the along-axis region of the shallow magma chamber reflectors, with a centroid position of 47°49′N (Johnson et al., 2000). Seismic activity migrated 12 km along axis at a rate of 1.1 km/h (Bohnenstiehl et al., 2004). Based on the character of the seismic events, increased CO_2 emissions from black smoker chimneys (Fig. 17), and pressure perturbations in Ocean Drilling Program Holes east of the ridge, the 1999–2000 event was interpreted to reflect diking beneath the ridge axis (Davis et al., 2001; Lilley et al., 2003; Seewald et al., 2003; Seyfried et al., 2003). The January 2000 swarm was more limited in extent, of shorter duration and did not show migration.

In contrast to the 1999 and 2000 swarms, the February 2005 swarm began at the overlapping spreading center on the northern end of the

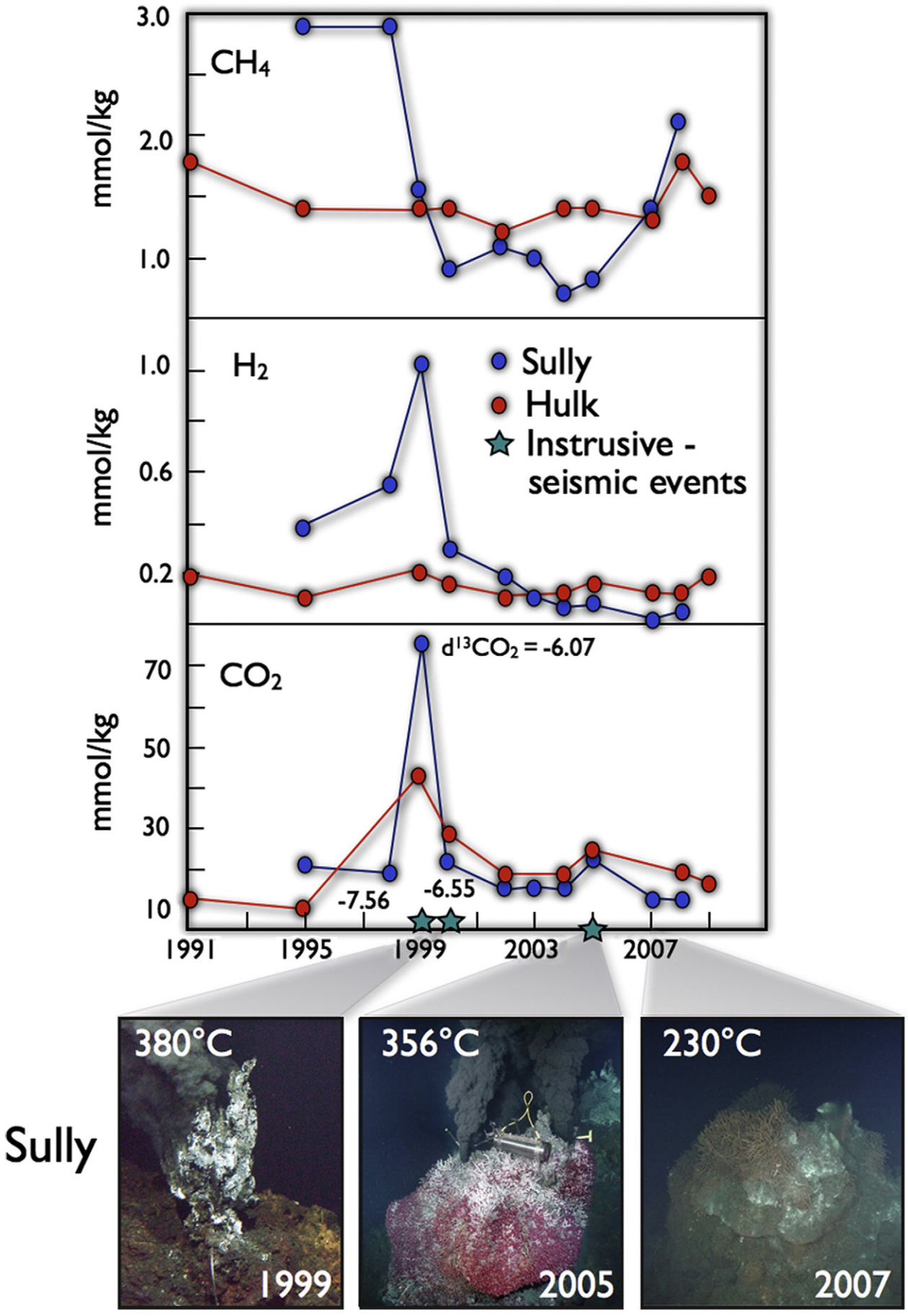
CH4
mmol/kg
3.0
2.0
1.0
H2
1.0
0.6
0.2
Sully
Hulk
Instrusive - seismic events
CO2
70
50
30
10
d13CO2 = -6.07
-7.56
-6.55
1991
1995
1999
2003
2007
Sully
380°C
1999
356°C
2005
230°C
2007

Endeavour Segment. It was the first event to be recorded by in situ battery-powered, short-period seismometers deployed in small boreholes and "seismonuments" at Endeavour as part of a UW-W.M. Keck Foundation proto-NEPTUNE experiment (Wilcock et al., 2009; Hooft et al., 2010; Weekly et al., 2013). In concert, these events perturbed the hydrology, chemistry, and biology of the Endeavour System, which had been relatively stable since the discovery of vents here in 1982 (Delaney et al., 1992; Lilley et al., 2003; Proskurowski et al., 2004; Hooft et al., 2010). They also resulted in hydraulic transients over 100 km east of the ridge, as recorded by pressure–temperature sensors in IODP drill holes (Davis et al., 2001).

From 2003 to 2004, the UW-Keck seismic network located 14,000 earthquakes on the Endeavour Segment. Approximately 4000 of these earthquakes occurred in the inferred position of the high-temperature portion of the reaction zone beneath the hydrothermal fields and just above the axial magma chamber reflector (Wilcock et al., 2009). The majority of the earthquakes lie in an arcuate band that extends from the High Rise Field to just south of the MEF. There is a remarkable correlation between the rate of seismicity beneath each vent field and their heat fluxes measured in the summer of 2004 (Wilcock et al., 2009; Kellogg, 2011). This suggests that the earthquakes are intimately linked to the processes of hydrothermal heat extraction, similar to the findings at the East Pacific Rise (Fornari et al., 2012).

Relative relocations and focal mechanisms for the Keck data suggest that the normal faults forming the axial valley graben extend down to near the axial magma chamber between the Main Endeavour and High Rise fields (Wilcock et al., 2009). The presence of earthquakes with compressional mechanisms to either side of the graben faults is consistent with a magma lens that is inflating (though no measurements similar to those at Axial have been made at this site). This led to the hypothesis that the high heat fluxes from the High Rise and Main Endeavour fields are driven by ongoing magma inflation that not only replenishes the magmatic heat source, but also cracks the carapace that would otherwise insulate the axial magma chamber (Wilcock et al., 2009).

In late January and late February 2005, the SOSUS arrays and the Keck network recorded two complex swarm sequences; 6000 earthquakes were recorded during this event (Hooft et al., 2010; Weekly et al., 2013). Each swarm involved a north to south progression of seismicity over several days between distinct clusters near West Valley and Endeavour Seamount, on the northern Endeavour Segment and in Endeavour Valley along the inferred extension of the West Valley propagator (Hooft et al., 2010; Weekly et al., 2013). The second swarm sequence was larger and led to an event response, which found no evidence for an eruption or water column perturbation (Dziak et al., 2007). The patterns of earthquakes recorded by the Keck network suggest that each sequence may have involved magmatic intrusions on the north Endeavour Segment and West Valley propagator, as well as deformation within the overlapping spreading center. Integrated Ocean Drilling Program borehole pressure records to the east of Endeavour suggest that the primary deformation associated with the late February sequence resulted from a dike intrusion on the northern Endeavour (Hooft et al., 2010). Interestingly, the migration of earthquakes suggests that the dike propagated southward toward the center of the segment from a magma source to the north, which is possibly associated with Endeavour Seamount at the east end of the Heck seamount chain (Weekly et al., 2013).

Both swarms triggered increased rates of seismicity beneath the vent fields that were delayed about two days from the onset of seismicity on the north Endeavour Segment. For the January swarm, the seismicity was concentrated between the Salty Dawg and High Rise fields (Weekly et al., 2013). The February swarm was concentrated further south between High Rise field and the MEF and coincided with a thermal perturbation to a diffuse vent site in the Mothra field (Hooft et al., 2010). Immediately following the swarm sequences and lasting until the end of the Keck deployment in 2006, seismicity almost ceased at both ends of the Endeavour Segment. Seismicity decreased to ~25% of pre-swarm levels beneath the vent fields (Weekly et al., 2013). It appears that the 2005 swarm marks the end of a 6-year episodic spreading event that cumulatively ruptured the entire segment and relieved the extensional stresses and magmatic pressures generating earthquakes (Weekly et al., 2013).

Similar to the RSN system, the ONC cabled array also/will include several short-period and broadband seismometers located within the rift valley and on the sedimented outer flanks (Fig. 18). Much of this array is located, or soon will be installed, at the same sites as the UW-Keck experiment (Wilcock et al., 2009; Hooft et al., 2010; Weekly et al., 2013). This seismic array is critical to maintain long-term investigations of diking events along the Endeavour and "imaging" of upflow zones. The seismic array coupled with temperature–chemical sensors will also allow better characterization of the hydrogeology of the Endeavour and linkages to changes in venting behavior: the seismicity in 2005 was concurrent with an ~4 °C rise in diffuse venting temperature in Mothra, and two thermal excursions at high temperature vents in the MEF (Hooft et al., 2010).

This seismic array is one of the few places in the world's oceans where fin whales can be tracked far offshore (Wilcock, 2012; Soule and Wilcock, 2012). The whales vocalize at 20 Hz. Between 2005 and 2006, 129,000 fin whale calls were detected with this network (Soule and Wilcock, 2012). The density distribution of the whale calls is not random, with some preference for localization about the Endeavour Segment. This has led to the hypothesis that the whales may be localized here because of enhanced zooplankton concentrations above the hydrothermal vents (Thomson et al., 1992; Soule and Wilcock, 2012). Instrumented water column moorings within the Endeavour axial rift, coupled with the seismic array will continue to test this hypothesis (Fig. 18).

3.2.2. Hydrothermal fields

The Endeavour Segment is one of the most hydrothermally active areas along the global MOR spreading system with numerous active and inactive chimneys densely concentrated over 15 km of ridge axis (Fig. 3b) (Delaney et al., 1997; Kelley et al., 2002, 2012). Indeed, analyses of 1-m resolution bathymetric data suggest that this portion of the segment may contain as many as 800 active and inactive chimneys (Clague et al., 2008). The central Endeavour Segment hosts five major discrete vent fields with spacing between fields increasing from about 1.5 km in the north, to 3 km to the south (Fig. 3b). Each of the major high-temperature fields extends over several hundred meters along-axis, and hosts multiple sulfide structures that are large compared to those at many slow- and fast-spreading ridges (e.g. Figs. 3b, 11c and 12b) (Delaney et al., 1992, 1997; Robigou et al., 1993; Kelley et al., 2001b, 2002; Glickson et al., 2007; Kelley and Shank, 2010). Venting has been long-lived at many of the fields (e.g., High Rise, MEF, Mothra) as evidenced by the massive sizes of the active chimneys (some are 50 m-across and 45 m-tall) and by extinct massive sulfide deposits that are 500 m in length (Fig. 11c). Endeavour is one of the few hydrothermally active areas globally where black smoker chimneys and extinct deposits have been dated. ^{226}Ra measurements indicate that

Fig. 17. Volatile chemistry for the hydrothermal edifices Sully (blue) and Hulk (red) located in the Main Endeavour Field. As illustrated, the hydrothermal systems in the Bastille complex, which hosts Sully, and the northern complex, which hosts Hulk, have continued to have distinct chemical–thermal properties both prior to and following the 1999–2000 events. The implication from these results is that the Bastille complex is fed by a different upflow limb of a convection cell than the northern complex (Fig. 11c). The appearance of isotopically heavy and radiocarbon dead CO_2 ($\delta^{13}CCO_2$) following the 1999 seismic event showed that the earthquake event was magmatic in origin (Proskurowski et al., 2004). Also shown is the evolution of macrofaunal communities on Sully, which has dramatically dropped in temperature since 2000 when it was venting 380 °C fluids.

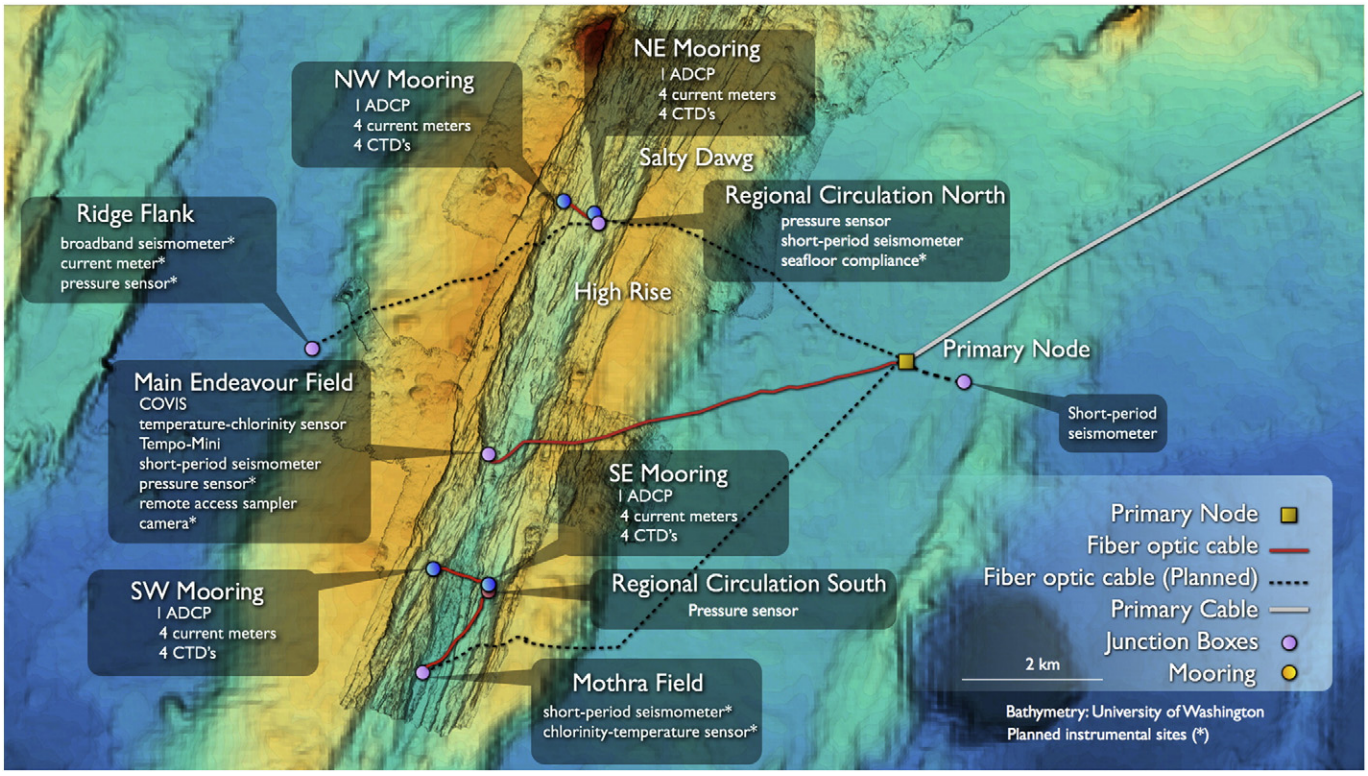

Fig. 18. Installed and planned cabled infrastructure at the central portion of the Endeavour Segment as part of the Ocean Networks Canada cabled system: installation is now complete. This system will provide co-registered time-series measurements (e.g. seismicity, vent fluid chemistry, temperature, and video imagery). The Endeavour array also hosts two sets of instrumented moorings that extend >200 m above the seafloor. Each mooring hosts acoustic Doppler current profilers (ADCPs), conductivity–temperature–depth sensors, and current meters.

hydrothermal activity has been active for at least 6000 years (Jamieson et al., 2013).

The MEF and High Rise Field are the most robustly venting systems along the segment, have the largest hydrothermal edifices, and historically have had the highest vent temperatures and most intense hydrothermal plumes (Fig. 16) (Butterfield et al., 1994; Delaney et al., 1992, 1997, 2001; Lilley et al., 1993, 2003; Robigou et al., 1993; Kelley et al., 2002): temperatures recorded in the MEF reached 402 °C in 1984 (Delaney et al., 1984). Within the MEF, in 1999–2000, there were 19 actively venting sulfide structures that hosted >100 individual black smoker orifices and the only white smoker complex on the segment (Cathedral; Fig. 11c).

The MEF area has been the focus of long-lived hydrothermal activity. About 100 m to the east of the present-day field, there is an extensive, ~500 m long linear deposit of massive oxidized sulfide and small chimney mounds. These deposits mark past venting sites that were clearly localized along a major 020-trending fault system subparallel to the fissure system currently feeding the MEF (Fig. 11c). It is thought that venting jumped to the present location of the MEF during a diking event, which then reorganized hydrothermal flow (Kelley et al., 2002). Sasquatch is the smallest field on the Endeavour with <10 active chimneys, while Mothra is the largest field, extending >600 m along axis and hosting at least six active sulfide complexes and greater than 50 sulfide structures (Figs. 3b and 16).

In addition to the major hydrothermal fields, there are also smaller sites of black smoker activity that include a small venting area south of Salty Dawg called Vesta, and the Raven Field, just north of the MEF (Fig. 3b). Less commonly, there are also present and past sites of black smoker activity on the western and eastern axial rift walls. For example, the Cirque site, located southwest of Salty Dawg at a water depth of ~2130 m, contains weakly venting 4–5 m tall black smokers, which in 1995 were venting 31 °C fluids (Fig. 3b). In 2006, extinct sulfides were recovered near the summit of the eastern valley wall northeast of Mothra. Numerous small extinct chimneys rise through the talus slope along the western rift wall at Mothra and within the Stockwork area, post-dating the talus (Kelley et al., 2012; Glickson et al., 2006).

The Endeavour Segment also hosts numerous sites of diffuse flow both proximal and distal to the high temperature fields (Fig. 13c and Table 1). The discrete distal sites from north to south include Dune, Clam Bed, Beach and Quebec. Clam Bed, south of High Rise is now a site of limited black smoker activity, perhaps in response to the increase in seismic activity at this site in 2005. In contrast to diffuse sites at the East Pacific Rise, which are sparse and only ~10 m × 10 m across, diffuse sites at Endeavour are numerous and commonly reach ~20 m × 50 m across or more (Table 1). The diffusely venting fluids, enriched in nutrients (e.g., CO_2 and $CH_4 \pm H_2$), support highly productive biological communities (Wankel et al., 2011). The higher frequency and abundance of both sulfide structures and diffuse flow sites at Endeavour versus Axial Seamount likely reflect the longer periods between eruptive events at Endeavour, which results in less disruption of the fluid flow paths, and longer periods before venting sites may be covered by lava.

In concert, the intense output of hydrothermal fluids along the Endeavour system forms extensive hydrothermal plumes (Fig. 16) (Dymond and Roth, 1988; Thomson et al., 2003; Veirs et al., 2006; Thomson et al., 2009; Kellogg and McDuff, 2010). The 2200-m deep axial rift valley and chemical–thermal properties of the hydrothermal fluids result in the development of intense buoyant plumes that rise to "trapping" depths as shallow as 1850 m (~350 m above the seafloor). The plumes spread laterally along the ridge axis by vent-induced circulation (Thomson et al., 2005). These neutrally buoyant plumes merge along axis and are significantly impacted by tidal currents above the ridge crest (Thomson et al., 2009). Results from sustained uncabled mooring deployments that "boxed in" the vent fields, coupled with

detailed along- and cross-axis CTD [conductivity–temperature–pressure (depth)] vertical casts, Tow' Yo's along-axis and high resolution 3D traverses with the autonomous vehicle ABE, integrated with modeling results, show that the buoyantly rising plumes create significant inflow of currents within the axial valley with equator-ward flow over the bounding ridge crests (Thomson et al., 2009). Plume-driven circulation within the axial valley may be important to biological processes by preferentially distributing larvae along axis- and more distally if they are entrained in the plumes that "escape" the valley and travel more than 10 km off-axis (Thomson et al., 2009).

To quantify plume activity and regional circulation at the central portion of the Endeavour Segment, two sets of two moorings (<300 m tall) are located within the axial rift north of the High Rise Hydrothermal Field and South of the Main Endeavour Field. Each mooring includes four CTDs and four current meters distributed along the vertical cable (Fig. 18).

3.2.3. Black smoker chimneys

The highest temperature hydrothermal chimneys at Endeavour commonly host thick rinds of chalcopyrite that line the inner conduits (Tivey and Delaney, 1986; Tivey et al., 1999; Kelley et al., 2002; Kristall et al., 2006, 2011). Though rarely directly measured, due to inaccessibility, conduits in the largest chimneys may reach several tens of centimeters across. Copper-rich minerals precipitate from the hottest hydrothermal fluids (generally greater than 250 °C). Other high-temperature minerals include iron and zinc sulfides (e.g., pyrite and sphalerite) (Tivey and Delaney, 1986; Tivey et al., 1999; Kristall et al., 2006, 2011). The outer walls of the chimneys are highly complex hosting multiple generations of smaller conduits, fractures, and complex stages of mineral paragenesis. Similar to chimneys at Axial, the walls are typically highly porous, and almost sponge-like in appearance. Here, ingress of seawater into the chimney walls results in variable mixtures of minerals directly precipitated from hydrothermal fluids (e.g., pyrite, sphalerite, chalcopyrite), and those largely derived from seawater that typically contain sulfate (e.g., barite and anhydrite) (Kelley et al., 2002). These systems are highly dynamic with myriad fracturing events within the chimney walls, changes in temperatures and chemistry of the upwelling fluids, and ingress of seawater (Tivey, 1995; Tivey et al., 1999; Kelley et al., 2002; Kristall et al., 2006). As the chimneys evolve, the pore space is commonly infilled with amorphous silica, adding strength to the chimneys and reducing permeabilities (Tivey and Delaney, 1986; Tivey et al., 1999; Kristall et al., 2006; Zhu et al., 2007). There is a systematic zonation in trace metals such as cobalt, cadmium, and uranium with implications for microbial habitats within the chimney walls (Kristall et al., 2011).

One of the hallmarks of the Endeavour black smoker edifices is the massive ledges, or flanges that grow from the chimney trunks, which reach sizes larger than the submersible *Alvin* (Tivey and Delaney, 1986; Delaney et al., 1992; Robigou et al., 1993; Kelley et al., 2002) (Fig. 12b). The flanges form when the walls of the black smoker edifices fracture and high temperature hydrothermal fluids rush out of the cracks and rapidly mix with seawater. Mixtures of hydrothermal fluids and seawater that flow through the top of the highly porous flanges support dense tubeworm and limpet assemblages (Figs. 12b and 13c). Nutrient-rich fluids within the flange walls support dense microbial growth (Hedrick et al., 1992; and Baross and Deming, 1995; Schrenk et al., 2003; Ver Eecke et al., 2009).

3.2.4. Perturbations within the fields

The 6-year spreading-diking event(s) along the Endeavour Segment has profoundly changed some of the vent fields since they were first discovered in 1982 (Delaney et al., 1992) (Figs. 16 and 17). Prior to 1999, there had been a long-standing chemical gradient between the northern and southern portions of the MEF interpreted to reflect feeding by two distinct upflow limbs (Butterfield et al., 1994; Delaney et al., 1997; Kelley et al., 2002). Fluid chemistry showed well-defined variation in salinity, carbon ($CO_2 + CH_4$) and temperature from north to south with the highest salinity, lowest temperature fields occurring at Sasquatch and Mothra (~300 °C, 710 mmol/kg Cl) and the highest total carbon concentrations in the north (Lilley et al., 1993; Butterfield et al., 1994; Delaney et al., 1997; Lilley et al., 2003).

The MEF held a long-standing record (two decades) for the highest measured vent fluid temperatures (up to 402 °C) (Delaney et al., 1984), with many of the structures in the southern Bastille complex exhibiting both boiling and supercritical condensation (Lilley et al., 1993; Butterfield et al., 1994; Delaney et al., 1997; Kelley et al., 2002; Lilley et al., 2003). However, the spreading event(s) and resultant seismic swarms disrupted this gradient and resulted in significant increases in gas concentrations, and profound changes in venting temperature, intensity, and chemistry. For example, the 1999 event caused dramatic, short-lived increases in CO_2 concentrations with isotopically heavy $\delta^{13}CO_2$ values down to −6.07‰ (Proskurowski et al., 2004), elevations in other magmatic gases, and elevated H_2 concentrations resulting from increased high-temperature water/rock reactions (Fig. 17) (Lilley et al., 2003; Proskurowski et al., 2004). The long-term high methane (CH_4) concentrations (up to 2.9 mmol/kg versus 0.12 mmol/kg for the bare rock system at 21 °N on the EPR), which were a hallmark of Endeavour hydrothermal fluids, showed a corresponding decrease. Elevated CH_4 concentrations, with highly depleted $\delta^{13}C$ values ($\delta^{13}CH_4 = -55‰$) at Endeavour are also associated with high ammonia concentrations. In concert, these relationships are thought to reflect the break down of organic material in sediments buried beneath the segment at an earlier stage in the ridge's evolution (Lilley et al., 1993). In some chimneys, such as Sully, the abundance and community composition of macrofaunal communities also changed significantly (Fig. 17), perhaps in response to changing H_2S concentrations and temperature. For example, in 1999, Sully was dominated by sea spiders (Pycnogonida), but by 2001 it hosted a vibrant community of tubeworms (*Ridgeia piscesae*): these were dying off by 2007 in association with significant lowering of fluid temperatures and weakening of hydrothermal discharge (Fig. 17).

Many chimneys within MEF increased temperatures by 15 °C with 380 °C temperatures being common. Both supercritical phase separation and boiling processes were active within many of the vents, and some orifices emitted fluids that were nearly "fresh" with respect to salinity (Lilley et al., 2003). Within MEF, new chimneys were initiated, flocculant material issued from the fissure systems, and many edifices sprouted several meters of new growth on their summits. Measurements at the MEF and Clam Bed site showed a tenfold increase in fluid output for at least 80 days following the event (Johnson et al., 2000). In contrast to this intense increase in hydrothermal activity during the 1999–2000 events, the southern Bastille complex (Fig. 11c), which had been venting 380 °C and nearly fresh fluids, is now dying with numerous chimneys only weakly venting (Figs. 12 and 17).

Hydrothermal plumes were also impacted by the spreading events. High Rise, as of 2005, had the highest heat flux of vent fields along the Endeavour Segment, and temperatures of some chimneys had increased (Kellogg, 2011) (Fig. 16). A significant plume was detected in 2005 above the Salty Dawg field that could not be sourced from either High Rise or Sasquatch (Kellogg and McDuff, 2010): some Salty Dawg vent fluid temperatures in 2006 increased from a previous visit in 2000. Activity at Sasquatch also increased since 2005; new chimneys developed, while others underwent dramatic growth (10 m in 1 year). In contrast, there were no changes in either vent fluid chemistry or black smoker temperatures at Mothra from 1996 to 2007; only weak seismic activity has been recorded beneath this field.

To constrain the relationships between diking and seismic events and hydrothermal processes, the ONC cabled array and instrumentation is focused predominantly at the MEF, with some instrumentation in Mothra (Fig. 18). Since 2010, black smoker and diffuse flow instrumentation have been focused on the black smoker called Grotto, located in the northern vent complex (Fig. 11c). A temperature–resistivity probe

is located within the throat of one of the 330 °C orifices on the sulfide deposit. A remote fluid sampler (similar to the one in the International District at Axial) has been measuring temperature and taking fluid samples in an adjacent diffuse flow area located on the side of Grotto (Fig. 6d and f). The fluid sampler is co-located with a video camera called Tempo Mini, designed by Ifremer in France (Fig. 6d and f). This novel system also includes an oxygen sensor, a colorimetric sensor to measure iron concentrations in the fluids, and a 10-m long, 10-sensor temperature array. Chemical and temperature analyses show that these systems are not only impacted by seismic events, but that hydrothermal flow is also impacted by lunar tides and local currents that waft up and down the rift valley (Tivey et al., 2002; Larson et al., 2009). One of the most advanced instruments within the MEF is called COVIS (Cabled Observatory Vent Imaging System) (Fig. 6e) (Bemis et al., 2012). This tripod-mounted sonar system is designed to image black smoker plumes issuing from Grotto as well as diffuse flow. It allows 3D volume images of the plumes, characterization of fluctuations in turbulence, and calculation of flow rates, volume flux and the areal extent of flow (Rona and Light, 2011). These instruments, coupled with moorings north and south of the fields, which box in the axial rift, will allow monitoring of plume development, evolution and heat flux.

4. Summary

Further advances in understanding MORs are increasingly dependant on our ability to collect long-term, high frequency observations using diverse networks of sensors and samplers. The major volcanic and tectonic events that create the oceanic crust and modulate fluxes from the seafloor to the hydrosphere are inherently episodic on decadal time scales and are also short-lived. It is also becoming increasingly clear that the effects of magmatic and tectonic events are not limited to the near field. Stress changes induced by fault motions and passage of seismic waves from distant earthquakes may trigger earthquakes and perhaps even volcanic eruptions. These punctuated events clearly perturb hydrothermal systems and their associated biological communities. The only way to capture these events is to maintain long-term monitoring capabilities at key sites with high probability for magmatic and tectonic activities.

The integrated high-power and high-bandwidth submarine cabled observatories at Axial Seamount and the Endeavour Segment will transform our ability to monitor and respond to processes active in these two dynamic environments. In concert, the instrument arrays at Axial and Endeavour, which will be fully deployed and operational in 2014, respectively, form the largest single in situ experiment in the global ocean focused on long-term measurements (25 years) of underwater volcanoes and the overlying ocean. Transmission of data and imagery back to shore is occurring in real-time and all data are/will be available to the public 24/7/365; both systems are highly expandable allowing rapid responses to new technological advances that include 4 K imaging, DNA 'on a chip' analyzers, and docked underwater autonomous vehicles with water column sensors, and seafloor and subseafloor imagers. The novel cabled infrastructure and contrasting attributes of Axial Seamount and the Endeavour Segment make these two sites ideal areas to achieve a major end goal in ridge-crest studies, which is to obtain co-registered transdisciplinary measurements at the required temporal and spatial scales that allow the development of quantitative, whole-system models with possible predictive capabilities. It is likely that profound discoveries will be made and new questions will both arise and be addressed as long-term data flow from these observatories.

Acknowledgments

The authors thank Dr. D. Piper for his invitation to contribute this paper to the 50th Anniversary issue of Marine Geology. The authors also thank D. Clague and an anonymous reviewer for their helpful comments that led to the improvement of this paper. We are grateful to the Center For Environmental Visualization team at the UW for their wonderful graphics and to M. Elend, also at the UW, for his painstaking efforts to produce remarkable mosaics of the seafloor. Support for this work was provided by the National Science Foundation, the UW, the University of Victoria, and Ocean Networks Canada.

References

Baker, E.T., Massoth, G.J., Feely, R.A., 1987. Cataclysmic hydrothermal venting on the Juan de Fuca Ridge. Nature 329, 149–151.
Baker, E.T., German, C.R., Elderfield, H., 1995. Hydrothermal plumes over spreading-center axes: global distributions and geological inferences. In: Humphris, S.E., Zierenberg, R.A., Mullineauz, L.S., Thomson, R.E. (Eds.), Seafloor Hydrothermal Systems; Physical, Chemical, Biological, and Geological Interactions. Geophysical Monograph, 91. American Geophysical Union, pp. 47–71.
Baker, E.T., Fox, C.G., Cowen, J.P., 1999. In situ observations of the onset of hydrothermal discharge during the 1998 submarine eruption of Axial Volcano, Juan de Fuca Ridge. Geophysical Research Letters 26, 3445–3448.
Baker, E.T., et al., 2004. Decay of hydrothermal output following the 1998 seafloor eruption at Axial Volcano: observations and models. Journal of Geophysical Research Letters 109. http://dx.doi.org/10.1029/2003JB002618.
Baker, E.T., et al., 2012. Hydrothermal discharge during submarine eruptions. Oceanography 25 (1), 128–141.
Baross, J.A., Deming, J.W., 1995. Growth at high temperatures: isolation and taxonomy, physiology, and ecology. In: Karl, D. (Ed.), The Microbiology of Deep-sea Hydrothermal Vents. The CRC Press, Inc., Boca Raton, Florida, pp. 169–217.
Baross, J.A., Hoffman, S.E., 1985. Submarine hydrothermal vents and associated gradient environments as sites for the origin and evolution of life. Origins of Life 15, 327–345.
Bemis, K., Lowell, R.P., Farough, A., 2012. Diffuse flow on and around hydrothermal vents at mid-ocean ridges. Oceanography 25, 182–191.
Bohnenstiehl, D.R., et al., 2004. Temporal and spatial history of the 1999–2000 Endeavour Segment seismic series, Juan de Fuca Ridge. Geochemistry, Geophysics, Geosystems 5, Q09003. http://dx.doi.org/10.1029/2004GC000735.
Butterfield, D.A., et al., 1990. Geochemistry of hydrothermal fluids from Axial Seamount Hydrothermal Emissions Study Vent field, Juan de Fuca Ridge: subseafloor boiling and subsequent fluid –rock interaction. Journal of Geophysical Research 95, 12,895–12,921.
Butterfield, D.A., et al., 1994. Gradients in the composition of hydrothermal fluids from the Endeavour Segment vent field: phase separation and brine loss. Journal of Geophysical Research 99, 9561–9583.
Butterfield, D.A., et al., 1997. Seafloor eruptions and evolution of hydrothermal fluid chemistry. Philosophical Transactions of the Royal Society of London 355, 369–386.
Butterfield, D.A., et al., 2004. Mixing, reaction and microbial activity in the sub-seafloor revealed by temporal and spatial variation in diffuse flow vents at Axial Volcano. In: Wilcock, W.S.D., DeLong, E.F., Kelley, D.S., Baross, J.A., Cary, S.C. (Eds.), Subseafloor biosphere at mid-ocean ridges. Geophysical Monograph Series, 144. American Geophysical Union, Washington D.C., pp. 269–290.
Carazzo, G., Jellinek, A.M., Turchyn, A.V., 2013. The remarkable longevity of submarine plumes: implications for the hydrothermal input of iron to the deep-ocean. Earth and Planetary Science Letters 66–76.
Carbotte, S.M., et al., 2012. Recent seismic studies at the East Pacific Rise 8°20′–10°10′N and Endeavour Segment: insights into mid-ocean ridge hydrothermal and magmatic processes. Oceanography 25 (1), 100–112.
Caress, D.W., et al., 2012. Repeat bathymetric surveys at 1-metre resolution of lava flows erupted at Axial Seamount in April 2011. Nature Geoscience 5, 483–488.
Chadwick Jr., W.W., et al., 1999. Evidence for deformation associated with the 1998 eruption of Axial Volcano, Juan de Fuca Ridge, from acoustic extensometer measurements. Geophysical Research Letters 26, 3441–3444.
Chadwick, J., et al., 2005. Magmatic effects of the Cobb hot spot on the Juan de Fuca Ridge. Journal of Geophysical Research Letters 110. http://dx.doi.org/10.1029/2003JB002767.
Chadwick Jr., W.W., et al., 2012. Seafloor deformation and forecasts of the April 2011 eruption at Axial Seamount. Nature Geoscience 5, 474–477.
Chadwick Jr., W.W., et al., 2013. The 1998 eruption of Axial Seamount: new insights on submarine lava flow emplacement from high-resolution mapping. Geochemistry, Geophysics, Geosystems 14 (10). http://dx.doi.org/10.1002/ggge.20202.
Clague, D.A., et al., 2008. Abundance and distribution of hydrothermal chimneys and mounds on the Endeavour Ridge determined by 1-m resolution AUV multibeam mapping surveys. Eos Transactions. AGU 89 (53) (Fall Meeting Supplement, Abstract V41B-2079).
Clague, D.A., et al., 2013. Geologic history of the summit of Axial Seamount, Juan de Fuca Ridge. Geochemistry, Geophysics, Geosystems 14 (10). http://dx.doi.org/10.1002/ggge20240.
Cowen, J.P., et al., 1999. Microbial biomass in hydrothermal plumes associated with the 1988 Axial Volcano eruption. Geophysical Research Letters 26, 3637–3640.
D'Asaro, E., Walker, S., Baker, E., 1994. Structure of two hydrothermal megaplumes. Journal of Geophysical Research 99, 20,361–20,373.
Davis, E.E., Elderfield, H., 2004. Hydrogeology of the Oceanic Lithosphere. Cambridge University Press 706.
Davis, E.E., et al., 2001. An episode of seafloor spreading and associated plate deformation inferred from crustal fluid pressure transients. Journal of Geophysical Research 106, 21,953–21,21963.
Delaney, J.R., Kelley, D.S., 2014. Next-generation science in the ocean basins: expanding the oceanographer's tool-box utilizing submarine electro-optical sensor networks.

In: Favali, P., Santis, A.D., Beranzoli, L. (Eds.), Seafloor Observatories: A New Vision of the Earth from the Abyss. Springer Praxis Books (in press).
Delaney, J.R., Johnson, H.P., Karsten, J.L., 1981. The Juan de Fuca Ridge-hot spot-propagating rift system: new tectonic, geochemical and magnetic data. Journal of Geophysical Research 86, 11,747–11,750.
Delaney, J.R., McDuff, R.E., Lupton, J.E., 1984. Hydrothermal fluid temperatures of 400 °C on the Endeavour Segment, northern Juan de Fuca Ridge. Eos Transactions AGU 65 (45) (Fall Meeting Supplement, 973).
Delaney, J.R., et al., 1987. Scientific rationale for establishing long-term ocean bottom observatory/laboratory systems. In: Teleki, P.G., Dobson, M.R., Moore, J.R., von Stackelberg, U. (Eds.), Marine Minerals Resource Assessment Strategies, pp. 389–411.
Delaney, J., et al., 1988. Scientific rationale for establishing long-term ocean bottom observatory/laboratory systems. The Mid-Oceanic Ridge — A Dynamic Global System, Proceedings of a Workshop. National Academy Press, Washington DC, pp. 234–257.
Delaney, J.R., Robigou, V., McDuff, R., 1992. Geology of a vigorous hydrothermal system on the Endeavour Segment, Juan de Fuca Ridge. Journal of Geophysical Research 97, 19,663–19,682.
Delaney, J.R., et al., 1997. The Endeavour hydrothermal system I: cellular circulation above an active cracking front yields large sulfide structures, "fresh" vent water, and hyperthermophile archaea. RIDGE Events 8, 11–19.
Delaney, J.R., et al., 1998. The quantum event of oceanic crustal accretion: impacts of diking at mid-ocean ridges. Science 281, 222–230.
Delaney, J.R., et al., 2000. NEPTUNE: real-time ocean and earth sciences at the scale of a tectonic plate. Oceanography 13, 71–83.
Delaney, J.R., et al., 2001. Edifice Rex Sulfide Recovery Project: analysis of a sulfide-microbial habitat from a submarine hydrothermal system. EOS. Transactions of the American Geophysical Union 82, 67–73.
Dymond, J., Roth, S., 1988. Plume dispersed hydrothermal particles: a time-series record of settling flux from the Endeavour Ridge using moored sensors. Geochimica Cosmochimica Acta 52, 2525–2536.
Dziak, R.P., Fox, C.G., 1999. Long-term seismicity and ground deformation at Axial Volcano, Juan de Fuca Ridge. Geophysical Research Letters 26, 3641–3644.
Dziak, R.P., et al., 2007. Rapid dike emplacement leads to eruptions and hydrothermal plume release during seafloor spreading events. Geology 35, 579–582.
Dziak, D.P., Hammond, S.R., Fox, C.G., 2011. A 20-year hydroacoustic time series of seismic and volcanic events in the Northeast Pacific Ocean. Oceanography 24 (3), 280–293.
Dziak, R.P., et al., 2012. Seismic precursors and magma ascent before the April 2011 eruption at Axial Seamount. Nature Geosciences 5, 478–482.
Einarsson, P., Brandsdottir, B., 1985. Seismological evidence for lateral magma intrusion during the July 1978 deflation of the Krafla Volcano in NE-Iceland. Journal of Geophysics 47, 160–165.
Embley, R.W., 1999. 1998 eruption of Axial Volcano: multibeam anomalies and seafloor observations. Geophysical Research Letters 26 (23), 3425–3428.
Embley, R.W., Baker, E.T., 1999. 1998 Interdisciplinary group explores seafloor eruption with remotely operated vehicle. Eos, Transactions American Geophysical Union 80, 213.
Embley, R.W., Murphy, K.M., Fox, C.G., 1990. High-resolution studies of the summit of Axial Volcano. Journal of Geophysical Research Letters 95, 12,785–12,812.
Embley, R.W., et al., 1991. Geology of the northern Cleft segment, Juan de Fuca Ridge: recent lava flows, sea-floor spreading, and the formation of megaplumes. Geology 19, 771–775.
Embley, R.W., et al., 2000. Recent eruptions on the CoAxial segment of the Juan de Fuca Ridge: implications for mid-ocean ridge accretion processes. Journal of Geophysical Research 105, 16,501–16,525.
Embley, R., et al., 2006. Long-term eruptive activity at a submarine arc volcano. Nature 441, 494–497.
Favali, P., Beranzoli, L., De Santis, A., 2014. Seafloor Observatories. Springer Praxis, United Kingdom 500.
Fornari, D., et al., 2004. Submarine lava flow emplacement at the East Pacific Rise 9°N: implications for uppermost ocean crust stratigraphy and hydrothermal fluid circulation. In: German, C.R., Lin, J., Parson, L.M. (Eds.), Mid-ocean ridges: hydrothermal interactions between the lithosphere and oceans. Geophysical Monograph Series, 148. American Geophysical Union, pp. 187–217.
Fornari, D.J., et al., 2012. The East Pacific Rise between 9°N and 10°N: twenty-five years of integrated, multidisciplinary oceanic spreading center studies. Oceanography 25 (1), 18–43.
Fox, C.G., Chadwick Jr., W.W., Embley, R.W., 2001. Direct observation of a submarine volcanic eruption from a sea-floor instrument caught in a lava flow. Nature 412, 727–729.
Glickson, D.A., Kelley, D.S., Delaney, J.R., 2006. The Sasquatch hydrothermal field: linkages between seismic activity, hydrothermal flow, and geology. Eos Transactions AGU 87 (52) (Fall Meeting Supplement Abstract V23B-0614).
Glickson, D.A., Kelley, D.S., Delaney, J.R., 2007. Geology and hydrothermal evolution of the Mothra Hydrothermal Field, Endeavour Segment, Juan de Fuca Ridge. Geochemistry, Geophysics, Geosystems 8 (6). http://dx.doi.org/10.1029/2007GC001588.
Gold, T., 1992. The deep hot biosphere. Proceedings of the National Academy of Science 89, 6045–6049.
Hammond, S.R., 1990. Relationships between lava types, seafloor morphology, and the occurrence of hydrothermal venting in the ASHES vent field of Axial Volcano. Journal of Geophysical Research 95, 12,875–12,893.
Harvey, J.B., 2012. Robotic sampling, in situ monitoring and molecular detection of marine zooplankton. Journal of Experimental Marine Biology and Ecology 413, 60–70.
Haymon, R.M., et al., 1991. Hydrothermal vent distribution along the East Pacific Rise crest (9°09′–54′N) and its relationship to magmatic and tectonic processes on fast-spreading mid-ocean ridges. Earth and Planetary Science Letters 104, 513–534.
Hedrick, D.B., et al., 1992. In situ microbial ecology of hydrothermal vent sediments. FEMS Microbial Ecology 101, 1–10.
Helo, C., et al., 2011. Explosive eruptions at mid-ocean ridges driven by CO_2-rich magmas. Nature Geoscience 4, 260–263.
Holden, J.F., Summit, M., Baross, J.A., 1998. Thermophilic and hyperthermophilic microorganisms in 3–30 °C fluids following a deep-sea volcanic eruption. FEMS Microbial Ecology 25, 33–41.
Hooft, E.E.E., et al., 2010. A seismic swarm and regional hydrothermal and hydrologic perturbations: the northern Endeavour Segment, February 2005. Geochemistry, Geophysics, Geosystems 11 (12). http://dx.doi.org/10.1029/2010GC003264.
Huber, J.A., Butterfield, D.A., Baross, J.A., 2003. Bacterial diversity in a subseafloor habitat following a deep-sea volcanic eruption. FEMS Microbiology Ecology 43, 393–409.
Huber, J.A., Butterfield, D.A., Baross, J.A., 2006. Diversity and distribution of subseafloor Thermococcales populations in diffuse hydrothermal vents at an active deep-sea volcano in the northeast Pacific Ocean. Journal of Geophysical Research 111. http://dx.doi.org/10.1029/2005JG000097.
Huber, J.A., et al., 2007. Microbial population structures in the deep marine biosphere. Science 318, 97–99.
Jamieson, J.W., et al., 2013. Sulfide geochronology along the Endeavour Segment of the Juan de Fuca Ridge. Geochemistry, Geophysics, Geosystems 14 (7). http://dx.doi.org/10.1002/ggge.20133.
Johnson, H.P., et al., 2000. Earthquake-induced changes in a hydrothermal system on the Juan de Fuca Ridge. Nature 407, 174–177.
Juniper, S.K., et al., 1994. Microbial–mineral floc associated with nascent hydrothermal activity at CoAxial Segment, Juan de Fuca Ridge. Geophysical Research Letters 22, 179–182.
Karsten, J., et al., 1986. Detailed geomorphology and neotectonics of the Endeavour Segment, Juan de Fuca Ridge: new results from Seabeam swath mapping. Geological Society of America Bulletin 97, 213–221.
Karsten, J.L., et al., 1990. Spatial and temporal evolution of magmatic systems beneath the Endeavour Segment, Juan de Fuca Ridge: tectonic and petrologic constraints. Journal of Geophysical Research Letters 95, 19,235–19,256.
Kashefi, K., Lovley, D.R., 2003. Extending the upper temperature limit for life. Science 301, 934.
Kelley, D.S., et al., 1998. Enriched H_2, CH_4, and ^3He concentrations in hydrothermal plumes associated with the 1996 Gorda Ridge eruptive event. Deep-Sea Research 11 (45), 2665–2682.
Kelley, D.S., Shank, T.M., 2010. Hydrothermal systems: a decade of discovery in slow-spreading centers. In: Rona, P.A., Devey, C.W., Dyment, J., Murton, B.J. (Eds.), Diversity of hydrothermal systems on slow-spreading ocean ridges. Geophysical Monograph, 188. American Geophysical Union, pp. 369–407.
Kelley, D.S., et al., 2001a. An off-axis hydrothermal field discovered near the Mid-Atlantic Ridge at 30°N. Nature 412, 145–149.
Kelley, D.S., Delaney, J.R., Yoerger, D.A., 2001b. Geology and venting characteristics of the Mothra Hydrothermal Field, Endeavour Segment, Juan de Fuca Ridge. Geology 29, 959–962.
Kelley, D.S., Baross, J.A., Delaney, J.R., 2002. Volcanoes, fluids, and life in submarine environments. Annual Review Earth and Planetary Science 30, 385–491.
Kelley, D.S., et al., 2005. A serpentinite-hosted submarine ecosystem: the Lost City Hydrothermal Field. Science 307, 1428–1434.
Kelley, D.S., et al., 2012. The Endeavour Segment of the Juan de Fuca Ridge: one of the most remarkable places on Earth. Oceanography 25 (1), 44–61.
Kellogg, J.P., 2011. Temporal and Spatial Variability of Hydrothermal Fluxes within a Mid-Ocean Ridge Segment. (Ph.D. Thesis) University of Washington.
Kellogg, J.P., McDuff, R.E., 2010. A hydrographic transient above the Salty Dawg hydrothermal field, Endeavour Segment, Juan de Fuca Ridge. Geochemistry, Geophysics, Geosystems 11 (12). http://dx.doi.org/10.1029/2010GC003299.
Kristall, B., et al., 2006. Growth history of a diffusely venting sulfide structure from the Juan de Fuca Ridge: a petrological and geochemical study. Geochemistry, Geophysics, Geosystems 7 (7). http://dx.doi.org/10.1029/2005GC001166.
Kristall, B., et al., 2011. Chemical microenvironments within sulfide structures from the Mothra hydrothermal field: evidence from high-resolution zoning of trace elements. Chemical Geology 290, 12–30.
Langmuir, C.H., Broecker, W., 2012. How to Build a Habitable Planet. Princeton University Press, Princeton New Jersey 734.
Larson, B.I., Lilley, B.I., Olson, E.J., 2009. Parameters of subsurface brines an hydrothermal processes 12–15 months after the 1999 magmatic event at the Main Endeavour Field as inferred from in situ time series measurements of chloride and temperature. Journal of Geophysical Research 114. http://dx.doi.org/10.1029/2008JB005627.
Lavelle, J.W., 1995. The initial rise of a hydrothermal plume from a line segment source — results from a three-dimensional numerical model. Geophysical Research Letters 22, 159–162.
Lavelle, J.W., Baker, E.T., Cannon, G.A., 2003. Ocean currents at Axial Volcano, a northeastern Pacific seamount. Journal of Geophysical Research 108. http://dx.doi.org/10.1029/2002JC001305.
Lilley, M.D., et al., 1993. Anomalous CH_4 and NH_4^+ concentrations at an unsedimented mid-ocean ridge hydrothermal system. Nature 364, 45–47.
Lilley, M.D., et al., 2003. Magmatic events can produce rapid changes in hydrothermal vent chemistry. Nature 422, 878–881.
Lupton, J.E., 1995. Hydrothermal plumes: near and far field. In: Humphris, S., Zierenberg, R., Mullineau, L., Thomson, R. (Eds.), Physical, chemical, biological, and geological interactions within seafloor hydrothermal systems. Geophysical Monograph, 91. American Geophysical Union, pp. 178–193.
Lupton, J.E., Baker, E.T., Massoth, G.J., 1999. Helium, heat, and the generation of hydrothermal event plumes at mid-ocean ridges. Earth and Planetary Science Letters 171, 343–350.

Lupton, J., et al., 2006. Submarine venting of liquid carbon dioxide on a Mariana Arc volcano. Geochemistry, Geophysics, Geosystems 7 (8). http://dx.doi.org/10.1029/2005GC001152.
Marcus, J., Tunnicliffe, Butterfield, D.A., 2009. Post-eruptive succession of macrofaunal communities at diffuse flow hydrothermal vents on Axial Volcano, Juan de Fuca Ridge, Northeast Pacific. Deep-Sea Research 11 (56), 1586–1598.
Martin, W., et al., 2008. Hydrothermal vents and the origin of life. Nature Reviews Microbiology 1–10. http://dx.doi.org/10.1038/nrmicro1991.
Massoth, G.J., et al., 1989. Submarine venting of phase-separated fluids at Axial Volcano, Juan de Fuca Ridge. Nature 340, 702–705 (1989).
McLaughlin-West, E.A., et al., 1999. Variations in hydrothermal methane and hydrogen concentrations following the 1998 eruption at Axial Volcano. Geophysical Research Letters 26, 3453–3456.
Meyer, J.L., et al., 2013. Microbiological characterization of post-eruption 'snowblower' vents at Axial Seamount, Juan de Fuca Ridge. Frontiers in Microbiology 4. http://dx.doi.org/10.3389/fmicb.2013.00153.
Murton, B.J., et al., 2006. Detection of an unusually large hydrothermal event plume above the slow-spreading Carlsberg Ridge: NW Indian Ocean. Geophysical Research Letters 33. http://dx.doi.org/10.1029/2006GL026048.
Nooner, S.L., Chadwick, W.W. Jr, 2009. Volcanic inflation measured in the caldera of Axial Seamount: implications for magma supply and future eruptions. Geochemistry, Geophysics, Geosystems 10 (2). http://dx.doi.org/10.1029/2008GC002315.
Opatkiewicz, A.D., Butterfield, D.A., Baross, J.A., 2009. Individual hydrothermal vents at Axial Seamount harbor distinct subseafloor microbial communities. FEMS Microbial Ecology 70, 413–424.
Proskurowski, G., Lilley, M.D., Brown, T.A., 2004. Isotopic evidence of magmatism and seawater bicarbonate removal at the Endeavour hydrothermal system. Earth and Planetary Science Letters 225, 53–61.
Proskurowski, G., et al., 2012. Post-eruptive time series hydrothermal contribution to the water column above Axial Seamount. EOS Proceedings of the American Geophysical Union OS22A-06.
Purser, A., et al., 2013. Temporal and spatial benthic data collection via an internet operated Deep Sea Crawler. Methods in Oceanography 5, 1–18.
Resing, J.A., et al., 2004. CO_2 and ^3He in hydrothermal plumes: implications for mid-ocean ridge CO_2 flux. Earth and Planetary Science Letters 226, 449–464.
Resing, J.A., et al., 2011. Active submarine eruption of boninite in the northeastern Lau Basin. Nature Geoscience 4, 799–806.
Robigou, V.R., Delaney, J.R., Stakes, D.S., 1993. Large massive sulfide deposits in a newly discovered active hydrothermal system, the High Rise Field, Endeavour Segment, Juan de Fuca Ridge. Geophysical Research Letters 20, 1887–1890.
Rona, P., Light, R., 2011. Sonar images hydrothermal plumes in seafloor observatory. EOS Transactions, American Geophysical Union. 92 (2), 169–170.
Rubin, A.M., Gillard, D., 1998. Dike-induced earthquakes: theoretical considerations. Journal of Geophysical Research 103, 10,017–10,030.
Scholin, et al., 2009. Remote detection of marine microbes, small invertebrates, harmful algae, and biotoxins using the environmental sample processor. Oceanography 22, 158–167.
Schrenk, M.O., et al., 2003. Incidence and diversity of microorganisms within the walls of an active deep-sea sulfide chimney. Applied and Environmental Microbiology 69, 3,580–3,592.
Seewald, J., Cruise, A., Saccocia, P., 2003. Aqueous volatiles in hydrothermal fluids from the Main Endeavour Field, northern Juan de Fuca Ridge: temporal variability following earthquake activity. Earth and Planetary Science Letters 216, 575–590.
Seyfried Jr., W.E., et al., 2003. Chemistry of hydrothermal vent fluids from the Main Endeavour Field, northern Juan de Fuca Ridge: geochemical controls in the aftermath of June 1999 seismic events. Journal of Geophysical Research 108. http://dx.doi.org/10.1029/2002JB001957.
Soule, D.A., Wilcock, W.S.D., 2012. Fin whale tracks recorded by a seismic network on the Juan de Fuca Ridge, Northeast Pacific Ocean. Journal of the Acoustically Society of America 133 (3), 1751–1761.
Summit, M., Baross, J.A., 1998. Thermophilic subseafloor microorganisms from the 1996 North Gorda Ridge eruption. Deep-Sea Research II 45, 2751–2766.
Summit, M., Baross, J.A., 2001. A novel microbial habitat in the mid-ocean ridge subsurface. Proceeding of the National Academies of Science 98, 2158–2163.
Thomson, R.E., et al., 1992. The deep scattering layer associated with the Endeavour hydrothermal plume. Deep Sea Research 39, 55–73.
Thomson, R.E., et al., 2003. Constrained circulation at Endeavour Ridge facilitates colonization by vent larvae. Nature 424, 545–549.
Thomson, R.E., et al., 2005. Numerical simulation of hydrothermal vent-induced circulation at Endeavour Ridge. Journal of Geophysical Research 110. http://dx.doi.org/10.1029/2004JC002337.
Thomson, R.E., Subbotina, M.M., Anisimov, V., 2009. Numerical simulation of mean currents and water property anomalies at Endeavour Ridge: hydrothermal versus topographic forcing. Journal of Geophysical Research Letters 114. http://dx.doi.org/10.1029/2008JC005249.
Tivey, M.K., 1995. The influence of hydrothermal fluid composition and advection rates on black smoker chimney mineralogy: insights from modeling transport and reaction. Geochemica Cosmochimica Acta 59, 1933–1949.
Tivey, M.K., Delaney, J.R., 1986. Growth of large sulfide structures on the Endeavour Segment of the Juan de Fuca Ridge. Earth and Planetary Science Letters 77, 303–317.
Tivey, M.K., et al., 1999. A model for growth of steep-sided vent structures on the Endeavour Segment of the Juan de Fuca Ridge: results of a petrologic and geochemical study. Journal of Geophysical Research 104, 22,859–22,883.
Tivey, M.K., et al., 2002. Insights into tide-related variability at seafloor hydrothermal vents from time-series temperature measurements. Earth and Planetary Science Letters 202, 693–707.
Van Ark, E.M., et al., 2007. Seismic structure of the Endeavour Segment, Juan de Fuca Ridge: correlations with seismicity and hydrothermal activity. Journal of Geophysical Research 112. http://dx.doi.org/10.1029/2005JB004210.
Veirs, S.R., McDuff, R.E., Stahr, F.R., 2006. Magnitude and variance of near-bottom horizontal heat flux at the Main Endeavour hydrothermal vent field. Geochemistry, Geophysics, Geosystems 7 (2). http://dx.doi.org/10.1029/2005GC000952.
Ver Eecke, H.C., Kelley, D.S., Holden, J.F., 2009. Abundances of hyperthermophilic autotrophic Fe(III) oxide reducers and heterotrophs in hydrothermal sulfide chimneys of the northeastern Pacific Ocean. Applied and Environmental Microbiology 75, 242–245.
Von Damm, K.L., 2000. Chemistry of hydrothermal vent fluids from 9°–10°N, East Pacific Rise: "time zero, " the immediate posteruptive period. Journal of Geophysical Research 105, 11,203–11,222.
Wankel, S.D., et al., 2011. Influences of subsurface biosphere on geochemical fluxes from diffuse hydrothermal vents. Nature Geosciences 4, 461–468.
Weekly, R.T., et al., 2013. Termination of a 6 year ridge-spreading event observed using a seafloor seismic network on the Endeavour Segment, Juan de Fuca Ridge. Geochemistry, Geophysics, Geosystems 14. http://dx.doi.org/10.1002/ggge.20105.
West, M., et al., 2001. Magma storage beneath Axial Volcano on the Juan de Fuca Ridge. Nature 413, 833–836.
Wilcock, W.S.D., 2004. Physical response of mid-ocean ridge hydrothermal systems to local earthquakes. Geochemistry, Geophysics, Geosystems 5 (11). http://dx.doi.org/10.1029/2004GC000701.
Wilcock, W.S.D., 2012. Tracking fin whales in the northeast Pacific Ocean with a seafloor seismic network. Journal of the Acoustical Society of America 132 (4), 2408–2419.
Wilcock, W.S.D., Archer, S.D., Purdy, G.M., 2002. Microearthquakes on the Endeavour Segment of the Juan de Fuca Ridge. Journal of Geophysical Research 107 (B12). http://dx.doi.org/10.1029/2001JB000505.
Wilcock, W.S.D., et al., 2004. The subseafloor biosphere at mid-ocean ridges. Geophysical Monograph, 144. American Geophysical Union, Washington, D.C., p. 399.
Wilcock, W.S.D., et al., 2009. The role of magma injection in localizing black smoker activity. Nature Geoscience. http://dx.doi.org/10.1038/NGE0550.
Zhu, W., et al., 2007. Permeability–porosity relationships in seafloor vent deposits: dependence on pore evolution processes. Journal of Geophysical Research 112. http://dx.doi.org/10.1029/2006JB004716.